REMOTE SENSING OF PRODUCTIVITY IN NORTHEASTERN FORESTS

A Thesis Presented

by

Aiko S.Weverka

to

The Faculty of the Graduate College

of

The University of Vermont

In Partial Fulfillment of the Requirements
for the Degree of Master of Science
Specializing in Natural Resources

October, 2012

Accepted by the Faculty of the Graduate College, The University of Vermont, in partial fulfillment of the requirements for the degree of Master of Science specializing in Natural Resources.

Thesis Examination Committee:

_____ **Advisor**
Jennifer Pontius, Ph.D.

_____
Gary Hawley, M.S.

_____ **Chairperson**
Shelly Rayback, Ph. D.

_____ **Dean, Graduate College**
Domenico Grasso, Ph.D.

Date: August 27, 2012

ABSTRACT

Remote sensing can provide a relatively low-cost and low-impact approach to large scale assessment of forest condition and productivity over time. However, the connection between canopy spectral signatures and scalable field metrics is not well understood. To explore this relationship, we compared annual basal area increment (BAI) at 47 sites throughout northern Vermont and New Hampshire to a suite of vegetation indices derived from annual growing season Landsat 5 TM imagery. Correlation analysis was used to evaluate the relationship between annual BAI and these indices at each site from 1984-2010, and a stepwise multiple linear regression model was created to predict BAI growth using a combination of multiple indices. Results showed weak significant relationships between BAI and several vegetation indices (mean $|\rho| = 0.104 \pm 0.032$) and that relationships between BAI and vegetation indices do not hold within most sites (<35%). The linear regression model created to predict BAI growth used a combination of four vegetation indices ($r^2 = 0.120$, $p < 0.0001$), although average residuals were high (mean standard error = 24.34) and significantly varied by species type ($p < 0.001$, $F = 58.07$).

These results indicates that while tracking relative changes in productivity is possible and more likely to be successful when species-specific, using remote sensing techniques for precise growth monitoring and accurate carbon accounting may be limited. The relationship between BAI, canopy characteristics and remotely sensed metrics at the plot level is likely nuanced, and complicated by heterogeneous species composition, variability in tree response to abiotic stressors, and the inability of single data imagery to characterize the quality of an entire growing season. While many have utilized remote sensing to quantify landscape scale productivity, the resulting coverages should be viewed conservatively.

ACKNOWLEDGEMENTS

I would like to thank my advisor Jen Pontius as well as the other members of my committee, Shelly Rayback and Gary Hawley, whose dedication and advice throughout the course of the past two years was indispensable. My research would not have been possible without the following people who helped me with field and lab work: Dylan Harry, Mike Olson, Kathryn Daly, Chris Hansen, Ben Engelman, Jon Schneiderman, Ali Kosiba, Kurt Schaberg, Katie White, and Alejandro del Peral. I would like to thank Ali Kosiba and Josh Halman for permitting me to use their tree-ring data and to everyone who helped them develop those datasets. I am also grateful to those who lent me equipment and lab space, and provided training including Paul Schaberg, Shelly Rayback, Joel Tilley, and Beverley Wemple.

Support for this project was provided by USDA National Needs Graduate Fellowship Competitive Grant No. 2008-38420-19547 from the National Institute of Food and Agriculture. This research was also supported by Northeastern States Research Cooperative.

TABLE OF CONTENTS

LIST OF TABLES

LIST OF FIGURES

CHAPTER 1: Literature Review

1.1. Forests in the Northeast

In the northeastern United States, forests are an important cultural, economic, and ecological resource. They provide recreational opportunities, non-timber forest products, and aesthetic beauty. Through direct forest-products manufacturing and forest-related tourism, they contribute approximately $19 billion annually to the economies of Maine, New Hampshire, New York and Vermont (North East State Foresters Association 2007). In addition to providing wildlife habitat, forests also perform crucial ecological services, including water filtration (Stein et al. 2009) and carbon sequestration (Goodale et al. 2002, Environmental Protection Agency 2010).

Forests in this region, however, also face an array of different stressors. Soil acidification associated with air pollution has been observed in the decline of certain species and the wider ecosystem (Driscoll et al. 2001). Established exotic insects and pathogens such as gypsy moth and beech bark disease, as well as newly invading pests such as the hemlock-woolly adelgid, emerald ash borer, and Asian long-horned beetle, are projected to have major effects on forested ecosystem processes (Lovett et al. 2006), with anticipated increases in frequency and severity of infestations and outbreaks (Allen 2009, Dukes et al. 2009). Increases in the frequency of severe weather events such as wind and ice storms (Dale et al. 2001) are predicted to lead to the decline of certain tree species, whereas changes in temperature and precipitation patterns may expand or limit the range of others (Iverson and Prasad 1998). Other studies, however, suggest that recent

widely observed forest declines are attributable to natural population senescence, as the majority of trees in the Northeast regenerated at roughly the same time (Wargo and Auclair 2000).

Given the presence of these different stressors, and concerns that forest mortality may be on the rise (Vermont Department of Forests 2010), monitoring is an important step in forest protection. Common forest monitoring methods include field-based studies and aerial surveys, but these are often limited by restricted scalability to the broader landscape and lack of temporal continuity (Zhang et al. 2011). Other potential methods of monitoring forests include dendrochronology studies and remote sensing.

1.2. Dendrochronology

Dendrochronology, the study of annual growth rings produced in trees, can be used to record environmental processes and monitor changes over time (Speer 2010). In temperate climates, trees produce new xylem tissue over a growing season that can generally be distinguished from previous and subsequent years' growth based on the color, size, and shape of cells that differentiate early wood (produced earlier in the growing season) and late wood (produced later in the growing season). This ring of xylem growth is known as a tree-ring. While the exact process that results in annual tree-ring production is not fully understood, environmental conditions appear to affect the level of growth hormones (e.g., auxin and cytokinin) that in turn regulate the initiation and rate of radial growth (Speer 2010). The width of a particular tree-ring can thus capture information about the environmental conditions during the growing season it was produced. This relationship between environmental conditions and tree-ring production

can be used to help monitor and quantify forest health by identifying the timing of specific disturbance events as well as more general tree stress levels given the relationship between prolonged reductions in radial growth and increased mortality risk (Wyckoff and Clark 2002).

Discrete disturbance events can be identified and placed in a larger context through the study of tree-ring patterns. In their research on pandora moth (*Coloradia pandora*) in Oregon, Speer et al. (2001) successfully developed an outbreak "signal," using knowledge of recent moth outbreaks, that was characterized by a precipitous reduction in ring-width that persisted for multiple years. With this outbreak signal, they identified similar occurrences over a 600+ year time span in 14 old-growth stands. The length and geographic scale of these tree-ring chronologies put recent pandora moth outbreaks in greater context and highlighted the potential role of historical processes and climate variation on the moth's population dynamics. Similar research identifying past pine beetle (Kulakowski et al. 2003), forest tent caterpillar (Sutton and Tardis 2007), and ciacada (Speer et al. 2010) outbreaks have been used to recreate the timing and relative severity of outbreaks.

Dendrochronology can also be used to identify specific occurrences of fire and drought. Swetnam and Baisan (1996), and Niklasson and Granström (2000) used burn scars present in tree-ring chronologies to reconstruct past fire history in the Southwestern United States and boreal Sweden respectively. Both of these studies revealed that the lack of fire in the region in the 20th century has been fairly anomalous and coincided strongly with historical land use practices. Stahle et al. (1998, 2007) compared tree-ring width to

modern precipitation and temperature measurements, and subsequently used this relationship to reconstruct nearly 800 years of drought occurrence history across North America. This long-term reconstruction illustrates the ability of tree-rings to track the spatial and temporal location of both short-term drought events (e.g., <5-10 year) as well as broader "megadrought" patterns that existed across wider geographical regions and for longer duration. Placing these discrete disturbance (e.g., insect outbreaks, fires) and meterological (e.g., drought) events into broader historical context allows for more nuanced interpretation of stressors that affect current forest health and productivity presently.

In addition to discrete disturbance events, dendrochronology can also be used to identify periods of long-term, more subtle, tree decline. Cherubini et al. (2002) examined the effects of two strains of fungal root pathogens on tree growth in mountain pine (*Pinus mugo*). While unable to time the exact onset of fungal infection, using patterns of tree-ring development they were able to identify which fungal strain was affecting each tree independent of phytopathological analysis. Findings from their study also suggest that it is possible to identify periods of tree decline using tree-rings many years before symptoms visible to the human eye arise or tree death occurs. Similarly, Duchesne et al.'s (2003) work on sugar maple (*Acer saccharum*) decline in Quebec found that decline in basal area increment preceded visual symptoms of decline by up to a decade . Their comparison of actual basal area increment relative to expected growth (independent of age-related trends) allowed them to record the initiation and duration of long-term reductions in growth, as well as pinpoint periods in which conditions worsened. This last

finding is particularly helpful to forest ecologists when studying areas where there is little recorded information about past disturbance history—a common occurrence for most forested regions.

In the Northeast, dendrochronology has been particularly used in the study of decline associated with acid deposition and winter injury. Local observations of red spruce (*Picea rubens*) decline since the 1960s and 1970s (Siccama et al. 1982) were shown to be quite widespread based on reductions in basal area increment measurements observed in 3,000+ trees cored in Vermont, New Hampshire, Maine, and the Adirondacks of New York in the 1960s-mid1980s relative to the previous 50 years (Hornbeck and Smith 1985). Research by Cook et al. (1987) using red spruce tree-ring widths and reconstructed climate records from these chronologies, suggested that these observed trends in growth reduction were not attributable to climate alone, implicating an external factor (i.e., air pollution and acid deposition). However, using these same climate reconstructions they also identified unusually cold winters as an inciting factor in red spruce decline. Similarly, work by Schaberg et al. (2011) examining the effects of a 2003 winter injury event found red spruce foliar dieback was significantly related to reductions in radial growth for multiple years. Notably, this work also identified trees with little evidence of foliar damage after the 2003 event that nevertheless had up to 31% reduction in radial growth. This hints at the complexity of environmental factors that influence growth and illustrates the cumulative effects of an entire growing season (and previous growing seasons) on final tree-ring width.

Halman et al. (2011) also examined the effects of a widespread winter injury event in the Northeast—the 1998 ice storm—on the crown vigor and radial growth of twelve paper birch sites. By measuring calcium depletion in soils at these sites, which has been shown to be linked to acid deposition from air pollution, they found there was a significant association between higher calcium concentrations and stronger recovery of both foliage and basal area increment following damage from that storm. Combining dendrochronology techniques with visual crown assessments and soil chemistry data provided a more nuanced and robust picture of paper birch health. Another study that examined forest response to the 1998 ice storm was Smith and Shortle's (2003) work measuring crown loss and radial growth of 347 hardwoods in New Hampshire and Maine. They found that while severe crown loss (>50%) led to significant immediate reductions in radial growth, most individuals showed signs of full recovery in tree-ring width by 2000. For some species (i.e., white ash (*Fraxinus americana*)), crown replacement occurred so quickly that the amount of crown loss in 1998 appeared to have no significant effect on measurements of radial growth 1998-2000. These studies illustrate how dendrochronology can be used to evaluate resiliency and recovery from disturbance, which is important both in the study of forest health as well as from a commercial timber management perspective.

Tree-rings have annual resolution and can provide decades, if not centuries of information about the status of an individual tree or stand, making dendrochronology very well-suited to monitoring forest condition changes over long periods of time (Biondi 1999). Although dendrochronology can provide a wealth of information about the long-

term health, resilience, recovery and/or decline of various forest ecosystems, collecting and processing cores can be a lengthy and tedious process that requires specialized equipment and training. Due to these processing requirements, dendrochronological studies are often limited in their geographic extent. Given these spatial limitations, dendrochronology can be paired with other tools to analyze forest health and productivity at a broader scale.

1.3. Remote Sensing of Forest Health and Productivity

In contrast to the highly detailed, yet localized information provided by tree-rings, remote sensing is a technique that can be used to monitor forests at the wider landscape scale and in areas where field work is not feasible. Remote sensing can be generally defined as "*...the science of acquiring information about the Earth's surface without being in contact with it. This is done by sensing and recording reflected or emitted energy and processing, analyzing, and applying that information*,"(Canada Centre for Remote Sensing 2007). The energy source most commonly utilized by aerial and space-borne remote sensing devices is the electromagnetic radiation emitted by the sun. This radiation, which has discrete contiguous wavelengths, travels from the sun and then interacts with the earth's atmosphere and surface features where it is scattered, transmitted, absorbed or reflected back to the sensor. Different features will interact with the different wavelengths in a unique manner depending on their physical properties and condition. For example plants reflect very little in the blue and red portion of the electromagnetic spectrum due to the presence of chlorophyll$_a$ and chlorophyll$_b$, which highly absorb wavelengths in in the blue and red range to power photosynthesis. In

contrast, blue light cannot penetrate water as effectively as longer wavelengths and is more highly reflected—hence the reason many bodies of water appear bluish to the human eye. Using knowledge of how various features interact with the electromagnetic spectrum, it is possible to classify and evaluate these features within larger images captured by the sensor. It is also possible to mathematically combine measurements of different wavelengths into ratios or other formulas to capture multiple pieces of information about a feature at once, while offsetting potential error associated with atmospheric attenuation and topography.

While there are a variety of sensors whose imagery can be used in remote sensing studies of forest health, imagery from the Landsat program is particularly well suited for this objective (Cohen and Goward 2004). The Landsat program has collected imagery nearly continuously since 1972 when the first sensor placed on a satellite platform for the purposes of studying and monitoring the earth's surface was launched by NASA. The scene size (183km swath) and temporal resolution (16 days) of images captured by Landsat program permit broad geographic and more detailed temporal coverage. Since 1982, with the launch of Landsat 4 Thematic Mapper (TM), spatial resolution has risen to moderate (30m) and the spectral resolution of imagery has expanded to 7 bands (3 visible, 1 near-infrared, 2 mid-infrared, and 1 thermal). Another major advantage to the use of Landsat data is that as of 2008, imagery is provided free-of-cost and is easily accessible.

Landsat imagery has been used to study and classify forest damage for a variety of tree types and stress events. Rock et al. (1986) found they could identify the relative

degree of damage (high v. low) to red spruce-balsam fir stands in northern Vermont with high accuracy (r^2 = 0.94-0.95) using a moisture stress index derived from Landsat 5 TM data. However, it remained ambiguous exactly what biophysical mechanism (e.g., water stress, cell structure, leaf biomass) was driving the observed differences in the imagery. Landsat 5 TM imagery has also been used to identify areas experiencing the initial stage of mortality (reddening of needles) associated with mountain pine beetle attack in British Columbia (Franklin et al. 2003). For the single year considered (1999), using a supervised classification with 360 ground truth points, Franklin et al. successfully distinguished attacked from non-attacked areas with 73% accuracy. Similarly, Nakane and Kimura (1992) utilized Landsat 5 TM imagery to map Japanese red pine (*Pinus densiflora*) blight. Using their model, they were able to correctly classify field sites to one of five damage classes 62% of the time, and to the correct or an adjacent damage class 96% of the time.

In addition to classifying and quantifying damaged areas from a single year, it is also possible to track changes in forests over time using Landsat imagery from different months or years. This is particularly useful when attempting to map damage extent, as it is possible to compare imagery pre-event to post-event imagery. In the Northeast, this type of analysis has been carried out by many researchers studying discrete disturbance events. In one of the earlier applications of Landsat TM technology for change forest detection, Vogelmann and Rock (1989) used imagery from 1984 and 1988 to identify deciduous forested areas affected by an outbreak of pear thrips *(Taeniothrips inconsequens*) in southern Vermont and western Massachusetts. Using ground-based

assessments and aerial sketch mapping they were able to estimate the degree of damage at the landscape scale from the Landsat imagery, however, it appears that no accuracy assessment was carried out to confirm their damage maps. Olthof et al. (2004) examined sugar maple damage in eastern Ontario caused by the severe region-wide 1998 ice storm using Landsat 5 TM images from 1996, 1997, 1998, and 1999. The percent crown lost due to storm damage was assessed at several training sites in and compared to raw Landsat bands and ratios pre- and post- storm. Using an independent set of sites where crown loss was also measured in the same manner as the training sites, their Landsat-based model had roughly 69% accuracy in distinguishing areas with severe damage from areas with light or moderate damage. Multi-year imagery has also successfully used to predict continuous, as opposed to discrete classes of defoliation. Townsend et al. (2012) compared the percent gypsy moth (*Lymantria dispa*) defoliation at several sites in northern Maryland to the degree of change in vegetation indices derived from 2000, 2001, 2006, 2007 and 2008 Landsat 5 TM images. Their resulting model had relatively high accuracy (r^2= 0.805, RMS error 14.9%) and they were able to apply the same model to a totally different system—aspen stands being defoliated by forest tent caterpillar in Minnesota—with apparent success based on visual comparison to sketch maps of that defoliation event. This illustrates the potential for expanding remote sensing forest monitoring techniques to new locations without always necessarily needing to invest in recalibration.

Due in part to the cost of obtaining Landsat imagery (prior to 2008) as well as the need for time-consuming image processing, there have been relatively few studies

that monitor forest condition over longer time scales than a few years. One example is the work done by Cohen et al. (2002) who used change detection on 11 years of Landsat images over a 23-year period (1972-1995) to identify areas associated with fire and harvesting activity in western Oregon. Given the relatively severe impact of fire and harvesting events on vegetation's spectral response, they were able to distinguish disturbed areas from non-disturbed areas with high (87.8%) accuracy. By combining these Landsat-based maps of forest disturbance with additional data, they tracked rates of disturbance over time as well as by land ownership patterns. Vogelmann et al. (2009) also studied forest condition over a long time period (1988-2006), but in this case were attempting to see more gradual changes in forest health, rather than abrupt disturbance from discrete events (e.g., fire or timber harvest). Using eight Landsat TM images over an 18-year period, they were able to track changes in reflectance over time and found significant declining forest condition trends in their study area in New Mexico. While no quantitative ground-truthing was carried out, inspection of the modeled declining areas suggested that insect defoliation and drought were likely contributing to the poorer spectral response observed in the imagery.

More recently Pontius et al. (in prep.) carried out similar research tracking overall forest health, as opposed to discrete disturbance events, over multiple decades. Using Landsat 5TM imagery from eastern New York, Vermont, and New Hampshire they assigned a continuous forest condition rating (0-10), based on five vegetation indices (using methodology developed in (Pontius in Review)), to each cloud-free pixel in a given year 1984-2009. The long-term trend of each pixel was then calculated as the slope

of the best fit linear trend line of those condition values plotted over time. Analysis of the resulting forest health trend model suggested that at the landscape scale, while there have been fluctuations in forest condition from year to year, overall there is no trend towards improvement or decline. At smaller scales, however, they found that there were localized patches of declining forest, much of which seemed to be associated with higher elevations and balsam fir- paper birch- red spruce communities (Olson 2011). However this model, like the one created by Vogelmann et al. (2009), has not be explicitly ground-truthed, making it difficult to gain a full picture of what ecological processes the Landsat imagery is recording.

Remote sensing studies designed to monitor forest condition over multiple years can be difficult to ground-truth, however, this is an important step given the complexity of processing remotely sensed images and the discrepancies between lab-findings and applications in the field (Hunt and Rock 1989, Pierce et al. 1990, Huete et al. 1994, Cunningham et al. 2009). There are few publically available, spatially explicit, long-term datasets that measure tree canopy condition, which is what the Landsat sensor is "seeing," over time. The Forest Inventory and Analysis (FIA) program, a forest health monitoring program administered by the US Forest Service and state agencies, seems like a logical data source to use for comparison to Landsat imagery given its extensive plot network and detailed collection of canopy condition, mortality, and regeneration data. The geographic coordinates of plot locations, however, are not available for research use and the data also lacks annual resolution as it is not possible to survey all plots every year. One way to work around this lack of past data when attempting to ground-truth

multi-year remotely sensed models of forest condition is to use tree-rings as a proxy for tree condition. Tree-rings have near annual resolution and can provide decades if not centuries of information about relative tree and stand health, depending on age. The preservation of this long-term information in the wood itself, also permits collection of long-term data at a single point in time.

1.4. Comparing Remote Sensing and Dendrochronology

The production of tree-rings is a complex process (Speer 2010), but there is field-based evidence that suggests the condition of foliage impacts tree-ring production (Smith and Shortle 2003, Halman et al. 2011, Schaberg et al. 2011) and that reduced radial growth is also associated with visual observations of foliar stress (Duchesne et al. 2003). Measurements taken by remote sensing devices also provide information about the condition of foliage given the different ways healthy and unhealthy vegetation interacts with the electromagnetic spectrum. Thus it is reasonable to hypothesize that there should be an observable relationship between these two metrics of forest condition—radial tree growth (tree-rings) and vegetation indices derived from remotely sensed imagery (see Figure 1 for the conceptual hypothesized relationship).

The relationship between forest productivity as measured by tree-ring increment and forest productivity as measured by remotely-sensed vegetation indices has been most intensely studied in boreal forests. One of the first studies to do this was carried out by Malmström et al. (1997) using net primary productivity (NPP) models that were created by combining mean meteorological data with NDVI measurements from Advanced Very

High Resolution Radiometer imagery (AVHRR). They compared tree-rings from a single site in Alaska dominated by birch and spruce to those NPP models 1982-1990, finding moderate positive correlations when comparing raw ring widths (r = 0.366-0.419) and strong correlations after detrending the tree-ring data (r =0.791-0.812). While this comparison was only carried out at one site (as a component of a larger study on productivity), the authors did highlight characteristics of tree-ring data they speculated would be most successfully correlated with NDVI. They suggest analyzed cores should be representative of the growth patterns, species composition, and age class distribution of all trees in the pixel of imagery the samples were collected in.

Using one of these same NPP models derived from NDVI over the same time period (1982-1990), D'Arrigo et al. (2000) came to similar conclusions when comparing maximum latewood density and tree-ring width to NPP at four sites in Alaska and Siberia. Correlation between NPP and a tree-ring width index was moderate to strong for all sites (r = 0.59-0.83), however, in this case detrending the tree-ring data actually lead to poorer correlation (r = -0.16- -0.19). Another interesting finding from this study was that the relationship between tree-ring metrics and NPP derived from NDVI was significant and strong in areas where the percent cover of the species cored was relatively rare (10%-63%). Based on their findings, the authors speculate that strongest relationship between tree-ring increment and NDVI will be observed in areas with a similar limiting growth factor for all species (e.g., temperature or water). This is because poor or strong growth of the species of interest will be mirrored by other (i.e., non-cored) vegetation, which also influences the signal received by the remote sensing satellite.

In 2004, the Global Land Cover Facility of the University of Maryland developed a multi-year bi-monthly model of NDVI 1981-2006, based on AVHRR imagery, with worldwide coverage known as the GIMMS (Gobal Inventory Modeling and Mapping Studies) NDVI dataset. With the creation of this dataset, it was possible to easily compare NDVI to tree-ring metrics without significant digital image processing requirements. This facilitated several more studies comparing NDVI to tree-ring data, again in boreal forests, with a focus of tracking these forests' responses to changes in climate. Comparing data 1981-2003, Kaufmann et al. (2004) found a significant robust correlation (r^2 = 0.68-0.91) between tree-ring increment and mean June, July and an integrated "growing season" NDVI value at 48 primarily-coniferous sites around the boreal region. In a similar study, Lopatin et al. (2006) cored Scots pine and Siberian spruce at five sites in northern Russia and found a significant overall correlation (r^2=0.44-0.59) between the standardized tree chronologies and NDVI summed June-August 1982-2001. This correlation, however, was statistically significant for four of the five Siberian spruce chronologies and only two of the four scots pine chronologies. Authors speculated that the lack of a significant relationship at certain sites may be attributable to spectral contributions from the understory, which presents more of a problem with narrow-crowned columnar trees.

Other studies comparing NDVI to tree growth in the boreal forest of the northern hemisphere also found a broad overall positive correlation, but that the relationship between tree-rings and NDVI fell apart for certain sites and species. Berner et al. (2011) cored 27 pine, spruce, and larch trees at sites in Canada and Russia and

found a consistently positive correlation between growing season NDVI (from the GIMMS dataset) and ring-width indices values (mean site $r = 0.43 \pm 0.19$). However, this positive correlation was only statistically significant at nine sites at the $p < 0.05$ significance level, and at fourteen sites at the $p < 0.10$ significance level. It also appeared that the strength of the relationship varied by site and by species, being weaker for larch-dominated areas. In addition, they found that there was no significant correlation between trends in NDVI and trends in ring-width index. That is, sites whose growing season NDVI increased 1982-2008 did not always show similar positive trends in the tree-ring index over the same period.

There have been relatively fewer studies comparing NDVI and tree-ring width in temperate forests. Wang et al. (2004) compared a tree-ring width index to measurements of NDVI from the GIMMS dataset over eight growing seasons (1989-1996) at a single oak-dominated site in Kansas. They found a very strong relationship ($r = 0.91$) between tree-rings and NDVI measurements averaged from mid-May to late June, however, this relation was weaker ($r = 0.76$) when comparing tree-rings to NDVI averaged over the entire growing season from late April to October. Expanding on their previous work from 2004, Kaufmann et al. (2008) considered the relationship between GIMMS NDVI measurements a tree-ring index at 101 sites, 53 of which were below 40ºN in latitude and dominated by deciduous species. Like Wang et al. (2004), they found a significant relationship to NDVI measurements from only certain portions of the year. In this case, ring width at these 53 sites was positively associated with NDVI measurements from April and May and was negatively associated with NDVI

measurements from October. This is in contrast to their findings that deciduous sites north of 40ºN had positive correlations with August NDVI, and conifers had positive associations with June and July NDVI. They speculate that variation in the relationship between tree-ring width and NDVI measurements from different months may be related to climate factors that affect growth.

Notably, all of these studies have been carried out using imagery that has coarse spatial resolution ranging from 8km to 1º degree (i.e., ~100km at northern latitudes). This means that NDVI measurements are very likely being averaged over a much larger area (64km^2-1,000km^2) than the area from which tree cores were collected to build a site chronology. Given the relatively homogeneous forest types found at northern latitudes, where the majority of the research comparing NDVI and tree-rings has been carried out, it is possible that cored sites were representative of enough of the surrounding landscape that the relationship was observable. Given the relatively short growing season boreal forests face, it is also possible that there are similar sources of environmental pressure (i.e., drought, cold temperatures) on multiple species that contribute to the NDVI signal recorded by the sensor. The potential influence from non-tree vegetation on NDVI is supported the work of Forbes et al. (2009) who studied the growth of willow shrubs in the Russian arctic. Comparing measurements of mid-July NDVI from the AVHRR dataset between 1981-2005 and ring widths from 15 site chronologies, they found a significant positive relationship ($r > 0.6$). However, the relationship between ring width and NDVI as measured in May and August was actually negative. This illustrates the

potential for shrubs to contribute to the NDVI signal, but also suggests that the variability of NDVI may make interannaul comparisons difficult, depending on imagery timing.

One of the few studies that has used imagery with moderate spatial resolution to derive NDVI estimates is the work carried out by Babst et al. (2010) on mountain birch in Sweden. In this complex study on the effects of autumnal moth (*Epirrita autumnata*) on tree-ring increment, they used three Landsat images (5TM and 7 EMT+) of three outbreak years and one Indian Remote Sensing Satellite (IRS) image in a year with no insect damage as a control. Comparing changes in NDVI between outbreak and normal years and changes in ring widths in outbreak and normal years for seven sites they developed a third degree polynomial regression model with an r^2 of 0.64. The imagery used in this study was high enough resolution (23m-30m) to capture disturbances that happen at smaller or patchier spatial scales, such as the defoliation caused by this moth outbreak. It is interesting to note they found the change in NDVI was linear to leaf area lost, but the radial reduction in growth was not. This disconnect between defoliation and reduction in radial tree growth hints at a potential complication in that Landsat may be better able to record more subtle decline than tree-rings.

1.5 Conclusions

A variety of stressors affect forests in the northeastern United States, and monitoring for these agents and the damage they cause is important in maintaining and improving forested ecosystem productivity in health. Satellite-based remote sensing is one technique that can be used to monitor forest health at the landscape scale, objectively, cheaply, and consistently. Landsat imagery is particularly well-suited to this task (Cohen

and Goward 2004). Recently Pontius et al. (in prep.) processed 27 years of Landsat imagery that covers eastern New York, Vermont, New Hampshire, and Maine. Using this imagery they were able to track changes in forest health using a newly developed vegetation index that is a combination of multiple hyperspectral indices adapted for multispectral imagery. This model as well as the suite of 49 additional vegetation indices derived from the same imagery 1984-2010, have yet to be ground-truthed to any metric of forest condition on the ground—a crucial step in assessing the limitations of a model.

Taking advantage of the relationship between environmental conditions/stress and radial tree growth, tree-rings have been used in a wide range of forest health studies throughout this region and the world. As tree-rings can provide long-term, nearly annual data they are a good source of information about past forest condition. This thesis research compares tree-ring data from 47 sites in Vermont and New Hampshire to vegetation indices derived from Landsat imagery to evaluate how well the latter corresponds to ground conditions of growth. Although previous authors have examined the relationship between radial growth and a single vegetation index (NDVI) with overall good (though varying) success, the majority of that research has been carried out in boreal forests with remotely sensed imagery that has much coarser spatial resolution than Landsat (Malmström et al. 1997, D'Arrigo et al. 2000, Kaufmann et al. 2004, Kaufmann et al. 2008, Forbes et al. 2009, Lloyd et al. 2010, Berner et al. 2011). Results of this research should provide more information about how well Landsat imagery can be used to monitor forest condition and productivity in temperate, Northeastern forests.

CHAPTER 2: Remote sensing of forest productivity in Northeastern forests

2.1. Introduction

Forests provide a range of goods and services including wood production and carbon sequestration. The ability of trees to perform these functions is dependent on many factors including water and nutrient availability, climatological factors, and both biotic and abiotic disturbances. Monitoring forests is a crucial step in ensuring forests remain biologically productive and meet desired management objectives (Ferretti 1997). Traditional approaches to long-term forest monitoring include repeated field assessments, but extrapolating these findings to the broader landscape scale can often be limited (Zhang et al. 2011). One monitoring technique that can provide landscape-scale coverage as well as new information at regular time intervals is satellite-based remote sensing.

Remotely sensed imagery has been used to study forest response to short-term disturbance events (Vogelmann and Rock 1989, Olthof et al. 2004, Townsend et al. 2012) as well as long-term trends in health and productivity (Cohen et al. 2002, Maselli 2004, Vogelmann et al. 2009, Pontius et al. in prep.). Many researchers have used imagery from the Landsat program in particular for this purpose given its moderate spatial resolution (30m), relatively high temporal resolution (16 days), large scene size (183km), low cost and deep historical record (1972-present) (Cohen and Goward 2004).

These studies often make use of vegetation indices, which are a combination of two or more reflectance values from different portions of the electromagnetic spectrum that reveals a particular property of vegetation, while reducing complications associated

with atmospheric interference and differences in illumination. The normalized difference vegetation index (NDVI), a combination of the red and near infrared portions of the electromagnetic spectrum, is one of the most commonly utilized vegetation indices and has been applied in the study of forest land use change, carbon storage, and biomass estimation (Maselli 2004, Myeong et al. 2006, Meng et al. 2009). There are many other vegetation indices designed for multi-spectral Landsat data that were developed to measure a range of features associated with forest condition including canopy water content (e.g., the moisture stress index (MSI) (Rock et al. 1986) and the normalized difference infrared index (NDII5) (Hunt and Rock 1989) as well as overall "greenness" (e.g., the enhanced vegetation index (EVI), the soil adjusted vegetation index (SAVI), and the simple ratio index (SR)).

More recently Pontius et al. (in Review) have taken a unique approach by adapting vegetation indices developed based on hyperspectral data and applying them to broadband Landsat data where possible. This approach takes documented narrow-band vegetation indices and uses the Landsat band containing the required wavelengths for index calculations. While much of the information contained in the narrow absorption features is lost in using the Landsat bands, the modified vegetation indices were found to be significantly associated with forest decline metrics (Pontius in Review). Using this methodology and summer growing season images they modeled forest decline in the Catskills region of New York, calibrated using a suite of canopy condition metrics (Pontius in Review). Across 11 distinct forest types, the resulting equation was able to predict a continuous 0-10 summary decline rating with $r^2 = 0.621$, RMSE = 0.403 and

jackknifed PRESS RMSE = 0.436. For comparison to more typical classifications of forest condition, this model predicted a 5-class condition with 100% accuracy (Pontius in Review).

Understanding what vegetation indices derived from remotely sensed imagery are telling us about conditions on the ground is crucial to its appropriate interpretation and application for monitoring and measuring purposes (Huete et al. 1994). There are many cases where it is not clear what the biophysical basis is for the relationship between a particular vegetation index and field observations of tree or stand condition (Hunt and Rock 1989, Pierce et al. 1990). Furthermore, relatively few of the hundreds of vegetation indices in existence have been widely tested across many forest types or over time. While ground-truthing is important in understanding what information Landsat imagery is actually providing and quantifying the accuracy of the coverages created, it is often difficult to carry out that process with historical studies given the need for accompanying field observations coincident with image acquisition.

One solution to the common lack of historical observations of canopy condition is to use another proxy for individual tree-health and productivity that is preserved from year to year in the trees themselves: annual xylem increment rings. Tree-rings have near-annual resolution and can therefore be used to assess radial growth retrospectively (Biondi 1999). They have been used as a proxy of forest productivity, and by extension forest health in many field studies throughout the Northeast (Siccama et al. 1982, Hornbeck and Smith 1985, Duchesne et al. 2003, Smith and Shortle 2003, Halman et al. 2011, Schaberg et al. 2011). Tree-rings have also been used to assess to multi-year

models of global productivity derived from remotely sensed imagery. This has been most widely carried out in boreal forests given interest in how trees in this region are responding to climate change (D'Arrigo et al. 2008). Several of these studies on boreal forests have found quite strong associations (r^2 up to 0.91) between metrics of tree-growth on the ground and the remotely sensed models. However it appears that these relationships do not always hold for all sites and species with remotely sensed imagery from certain portions of the year.

The purpose of this research was to study the relationship between radial tree growth (tree-rings) and vegetation indices derived from Landsat 5 TM imagery in northeastern forests. The following questions were investigated:

1. Is there a relationship between measurements of basal area increment and vegetation indices derived from Landsat 5 TM data the same year 1984-2010?
2. If these relationships exist, are they stronger for certain vegetation indices, species types, or particular locations?
3. Is there some combination of multiple vegetation indices that can be used to model BAI across the landscape?

Given the potentially broad applications of remote sensing technology for forest health monitoring (Franklin 2001) and carbon accounting, it is important to examine how well remotely sensed metrics of forest canopy characteristics relate to measurements of tree growth on the ground. While there have been multiple studies comparing NDVI to tree-rings (D'Arrigo et al. 2000, Kaufmann et al. 2004, Lopatin et al. 2006, Forbes et al. 2009, Lloyd et al. 2010, Berner et al. 2011), there is limited research on temperate forests

(Wang et al. 2004, Kaufmann et al. 2008) and most previous studies, with a few exceptions (Babst et al. 2010), utilize imagery with coarser spatial resolution (1km-8km pixel size). This study should provide an opportunity to examine the relationship between vegetation indices and radial tree-growth in a more heterogeneous forested ecosystem using more spatially precise imagery. The resulting methodologies will describe the "best" approach for modeling forest productivity using multi-spectral imagery, as well as a better understanding of the accuracy and limitations of using remote sensing to assess forest growth.

2.2. Methods

2.2.1. Study Sites

In order to capture forest growth rates across a range of species, decline condition and land use histories, we used data from 47 plots throughout northern Vermont and New Hampshire (Table 1) (Figure **2**). Falling across a broad elevational gradient (96 m-1155 m above sea level), plots were dominated by red spruce (*Picea rubens*), balsam fir (*Abies balsamea*), paper birch (*Betula papyrifera*), yellow birch (*Betula alleghensis*), red maple (*Acer rubrum*), sugar maple (*Acer saccharum*), American beech (*Fagus grandifolia*), white pine (*Pinus strobus*), and red pine (*Pinus resinosa*). Of the 47 sites, 16 were established in summer 2011 to capture a broad range of long-term canopy condition trends predicted by a remote sensing forest health model (Pontius et al. in prep.). To increase the sample size and robustness of findings, 31 pre-existing sites from research conducted by Halman et al. (2011) in fall 2006, and Kosiba et al. (in

review) in fall 2010, on paper birch and red spruce, respectively were also included in analysis.

2.2.2. Dendrochronology

At each study site two xylem increment cores were collected at ~180º from 4-20 co-dominant trees present within a ~15-30m radius of plot center. At the Halman and Kosiba sites, only red spruce and paper birch were sampled, while up to up to three dominant tree species were sampled at the 2011 sites (

Table 1). Cores were dried, mounted and sanded, according to standard procedures (Stokes and Smiley 1968) and visually cross dated using the list method (Yamaguchi 1991). We then measured each core using a Velmex sliding stage (Velmex Inc., Bloomfield, NY) to the 0.001 mm level using J2X software (VoorTech Consulting, Holderness, NH). Statistical cross-dating was carried out using COFECHA (version 6.06) to verify and improve dating accuracy (Grissino-Mayer 2001, Speer 2010). Although cores were collected by different groups (Halman, Kosiba, Weverka), all processing steps were similar and much of the cross-dating was carried out using the same equipment and technicians.

Once cross-dated, we converted raw measurements into annual basal area increment (BAI) (mm^2/year), assuming a perfectly circular tree, using diameter at breast height (DBH) measurements. BAI was used instead of a ring-width index to facilitate comparison across multiple species and account for the fact that rings become smaller as a tree's radius increases due to geometric properties (Speer 2010). To come up with a single annual BAI measurement for each site, the two cores from each tree were

averaged, and then all trees at each site were averaged. In cases where multiple species had been sampled at a site, we used species basal area (calculated using DBH field measurements of all trees > 12.5 cm diameter in a 17m radius plot) to calculate a weighted average BAI.

2.2.3. Remote Sensing

In order to compare field measured BAI at each plot, to spectral reflectance metrics, imagery from the Landsat 5 Thematic Mapper (TM) sensor was obtained from the US Geological Service Global Visualization Viewer (http://glovis.usgs.gov/). For each of the 27 years imagery is available (1984 – 2010) we downloaded one growing-season (i.e., June 10-August 20) image for two Landsat scenes covering our study area: Row 29-path 13 (Vermont/ New Hampshire) and row 29-path 14 (eastern New York/Vermont) (Table 2). A single growing-season image was deemed sufficient to capture the spectral characteristics of that year's vegetation based on previous findings that foliar chemistry and associated reflectance values remain fairly stable after initial leaf-out in temperate forests (Martin 1994, Bauer et al. 1997). Due to consistent cloud cover, there was one year (1995) where no imagery was available for both Landsat scenes. On a site by site basis, there were often multiple years (up to 16 years) of missing data due to partial cloud cover.

Landsat level 1T imagery includes a radiometric correction using the revised calibration gains for the reflective bands 1–5 and 7 (Chander et al. 2009) and a preliminary orthorecification. In order to control for inherent differences between Landsat images acquisitions that were not related to changes in canopy reflectance,

several additional processing steps were required to normalize reflectance across the imagery time series. We first converted raw digital number (DN) values to top of atmosphere reflectance to account for differences in illumination intensity and sun angle among acquisition dates using ENVI 4.8 (Exelis 2011, Colorado Springs, CO). Calculation of many of the vegetation indices explored in this study required an additional conversion to at-surface reflectance. We chose a histogram-based dark object subtract for each band. This dark object subtract approach has been shown to be as effective at reducing the differences in surface reflectance estimation between multi-date images as more complex radiative transfer models for multi-spectral imagery (Song et al. 2001). To ensure accurate co-registration of pixels across years, we georegistered each image to a common mid-study cloud-free image using a 3^{rd} order polynomial with a nearest-neighbor resampling technique (root-mean square error < 0.2 pixels or 6m average accuracy). Considering the 17m radius field plots and 30 m spatial resolution of the Landsat sensor this level of accuracy is necessary to ensure correct spectra extraction for each field plot.

Surface reflectance was extracted for bands 1-5, and 7 using the Spatial Analyst tools in Arc 10 (ESRI 2011, Redlands, CA) from the closest pixel to the GPS coordinates of plot center. Cloud cover, haze, and cloud shadow can "pollute" reflectance values as they mask and alter spectral data. To ensure that only cloud free data was included in our analysis we visually inspected each site across all images. Extracted values were manually converted to "NoData" for that year if the site was covered by cloud, cloud shadow or visible haze in any given image. Given that the two Landsat scenes included in

this study overlap for ~65 km across New Hampshire and Vermont (Figure 2), there were many study sites with two sets of spectral data available in each year. Where available, these spectral values were averaged to come up with one set of spectral data per year.

While Landsat band locations were developed with vegetation applications in mind, there is a wealth of vegetation indices that can improve upon the ability of the sensor to detect specific canopy biophysical parameters (Table 3). This includes many broad-band indices, designed specifically using multi-spectral sensors like Landsat, but also extends to a suite of narrow-band indices designed specifically for hyperspectral applications, that to our knowledge have not been tested using broad-band sensors.

In order to conduct a comprehensive assessment of Landsat's ability to quantify forest growth and productivity, we created a spectral database to calculate a suite of vegetation indices with documented relationships to canopy characteristics. For narrow-band indices, we calculated a Landsat equivalent where each distinct narrow-band wavelength required for calculation fell within a distinct Landsat band. For example, the chlorophyll sensitive index proposed by Datt (1998) calls for a ratio between reflectance at 672 nm and R550 nm. We calculated a broad band equivalent as Landsat 5 TM Band3:Band2. While the expectation is that much of the specific information pertinent to $chlorophyll_b$ content captured in the narrow-band equation will be lost in the broad-band equivalent due to the narrow $chlorophyll_b$ absorption feature, there may still be enough information relative to vegetation condition to make it useful in a more complex model. The resulting database calculated 55 pre-existing vegetation indices/raw bands (Table 3) including common multi-spectral indices such as the normalized difference vegetation

index (NDVI), and more complex narrow-band indices like the structure insensitive pigment index (SIPI).

2.2.4. Statistical Analysis

As a preliminary data exploration step, annual BAI measurements were compared to annual vegetation indices across all sites and all years 1984-2010 (n =701) using Spearman's rho correlation. While statistically complicated by temporal autocorrelation, and artificially inflated sample size, this analysis was not intended to identify significant relationships, but instead to identify which of the 55 vegetation indices were likely to have a significant relationship with BAI in subsequent analyses. This was of considerable interest based on our goal to develop a global, or "landscape scale," model to quantify forest growth. Such a model would have to maintain relationships across sites of varying species composition and years of varying growth conditions. To explore the strength of fit when analysis was limited to a single species, this test was rerun on 5 species "types"("Red Spruce," "Birch," "Pine," Mixed Hardwoods," and "Mixed Balsam Fir/Red Spruce/ Birch") that were created by combining data from sites with similar species composition.

To measure the relationship between BAI and vegetation indices while accounting for inherent differences in tree-ring series (as a result of different species composition, landscape characteristics, external disturbance etc.) and autocorrelation across years (Berner et al. 2011), we conducted a Spearman's rho correlation across all available imagery years on a site by site basis. Correlation analysis assumes independence among observations—a condition likely to be unmet by tree-ring data

given the effect one year's growth may have on subsequent years. To address the statistical violation of carrying out correlations on datasets with potential temporal autocorrelation across years, the effective sample size was reduced by penalizing the sample size in proportion to the degree of first order autocorrelation between one year's BAI and the following year's BAI (Dawdy and Matalas 1964 adapted by Berner et al. 2011; Appendix A) in R (version 2.15.1). In cases where there was no significant ($p < 0.05$) autocorrelation, the full sample size was preserved. This site-specific analysis also highlights which types of stands have the strongest or weakest relationships between BAI and vegetation indices, or if different indices are required to quantify growth in different forest types. Due to cloud cover present in the imagery, not all years were available at all sites, further limiting the sample size.

Because woody growth is potentially related to many different canopy metrics (leaf area index, chlorophyll content, leaf moisture content, etc.) it is possible that no single spectral index can be used to quantify forest growth alone. To test this theory, we developed a multi-vegetation index model to predict forest growth across the region (i.e., with data from all sites and all years) using stepwise linear regression. With BAI as the dependent variable, the mixed platform tests all possible linear regressions combinations, retaining vegetation indices that strengthen the model fit. To avoid over-fitting, model development was limited to a maximum of 5 terms (Williams and Norris 2001), $\alpha < 0.05$ for all terms and a variance inflation factor < 10 (Kleinbaum et al. 1998). Jackknifed residuals calculated from the PRESS statistic were also used to assess the stability of the final predictive equation (Kozak and Kozak 2003). Based on preliminary results, an

analysis of variance with a Tukey HSD post-hoc test was run on the model's residuals and it appeared that there was a significant species effect. Consequently this analysis was also carried for each of the 5 species "types."

All analyses were carried out in JMP 9.0 (SAS Institute Inc., Cary, North Carolina).

2.3. Results and Discussion

2.3.1. Global Correlation Data Exploration

Comparing BAI and vegetation indices across all years and all sites revealed fourteen vegetation indices that had significant ($p \leq 0.05$) relationships with BAI measurements (Table 4). NDVI, one of the most commonly used vegetation indices in studies comparing remotely sensed data and tree-rings (Kaufmann et al. 2004, Lopatin et al. 2006, Kaufmann et al. 2008, Forbes et al. 2009, Babst et al. 2010, Lloyd et al. 2010, Berner et al. 2011) was not significantly correlated to BAI ($\rho = - 0.055$, $p = 0.1389$). Notably, however, the soil adjusted and atmospherically resistant vegetation index (SARVI) was significantly related ($\rho = 0.077$, $p = 0.0409$). SARVI is very similar to NDVI in what biophysical parameters it is designed to measure (Leaf Area Index, % green cover, green biomass, and absorbed photosynthethically active radiation) (Huete et al. 1994). The difference between NDVI and SARVI is that the latter is adjusted to offset contamination from soil brightness and atmospheric interference. Mathematically this is accomplished by normalizing blue reflectance (band 1) and including a constant to adjust for soil brightness, as opposed to NDVI, which is only calculated using the red and near

infrared (Bands 3 and 4) (Table 3). This built-in adjustment for atmospheric and soil interference may help explain why SARVI had a stronger relationship to BAI than NDVI.

Of the remaining thirteen vegetation indices that were significant, three were indices designed for multispectral data (MSI, NDII5, NDII7), eight were adapted from hyperspectral indices for Landsat TM data (NPCI, SIPI, SRPI, MSR705, MND705, HAM, Flo, VogB) and two were the raw Landsat bands: band 5 and band 7 (Table 4). These two raw bands, as well as the moisture stress index (MSI), and the two normalized difference infrared indices (NDII5 and NDII7) are sensitive to water stress (Vogelmann and Rock 1988, Hunt and Rock 1989). Indices that record a water stress signal may have a stronger relationship to measurements of BAI because drought is a relatively non-specific and non-fatal stress event. Unlike other stressors that target specific tree species or age classes (e.g., insect outbreak, storm damage), or occur rarely in our chronology, drought elicits a more general response. Climate events also occur beyond the scale of a single stand and so the fact that a broader portion of the landscape is likely to be responding to the same stressor may help account for any geographic inaccuracies in the Landsat data (D'Arrigo et al. 2000). Lastly, given that water stress in the Northeast is rarely prolonged enough to cause mortality, it is also likely trees will survive to carry a record of the event in their rings, as opposed to dying off before sites were cored in 2006 and 2010.

Seven of the remaining significant vegetation indices were developed to measure chlorophyll content (VogB) (Vogelmann et al. 1993), chlorophyll fluorescence (Flo) (Mohammed et al. 1995) or the ratio of total pigments and carotenoids to

chlorophyll (NPCI, SIPI, SRPI, MSR705, MND705) (Peñuelas et al. 1993, Peñuelas et al. 1995, Sims and Gamon 2002). Chlorophyll levels are related to a plant's ability to produce carbohydrates and by extension the xylem tissue that forms tree-rings. Chlorophyll fluorescence can be used as an early indicator of leaf stress as it is one of the first indicators of reductions in photosynthetic efficiency (Maxwell and Johnson 2000). Higher ratios of carotenoids to chlorophyll is also indicative of stress (Peñuelas et al. 1995, Sims and Gamon 2002) as the relative concentrations of carotenoids tends to rise and persist longer than chlorophyll in unhealthy plants.

The final vegetation index with a significant relationship to BAI was the hyperspectral adapted to multispectral (HAM) index developed by Pontius et al (in Review). This HAM index is a mathematical combination of multiple vegetation indices, calibrated to field measurements of canopy condition, designed to provide an overarching assessment of canopy condition across species types. Given that it contains three of the vegetation indices found significant in this analysis (SIPI, Flo, Band 5) it is perhaps not surprising that it also emerged as being significantly related to BAI in our global analysis.

Despite logical explanations for why these particular vegetation indices have a significant relationship to BAI, it is important to note that these relationships were all quite weak with the absolute value of the Spearman-rho coefficient ranging from 0.0719 to 0.157. This is lower than other similar studies. For example in their study comparing NDVI to ring-widths to 22 sites in Siberia and Canada (Berner et al. 2011), the overall mean Pearson product moment correlation value (r) was 0.43. Likewise Forbes et al. (2009) found a stronger association ($r = 0.6$), when comparing mid-summer NDVI to

tree-ring width index of willows at 27 sites in northern Russia. There are many experimental and ecological explanations for the observed relatively low correlation coefficients, many of which are discussed in section 2.3.4. While these overall associations are relatively weaker, our results show that other vegetation indices outperformed the commonly used NDVI, suggesting that future studies using remote sensing techniques to quantify forest growth should consider expanding the range of indices utilized.

At this "global" scale, plotting out BAI against each significantly correlated vegetation index and color coding data points by species membership (for an example, see Figure 3) also revealed that there are distinct species clusters, which suggests significant variation in the relationship by species. Re-running this same analysis for each species type (i.e., the same analysis, but only using data that fell into sites dominated by that particular type) resulted in more vegetation indices having a significant relationship to BAI measurements for some species types (Birch, Red Spruce, Mixed Hardwoods) (Table 5), and stronger absolute ρ values (ρ = 0.135-0.564) for all species types. Many of the indices found significant in the initial global correlation (i.e., data from all sites) were also found significant in these species type correlation analyses. These findings suggest comparing radial growth with remotely sensed metrics of forest condition are more likely to be successful if species-specific adjustments are made. Possible explanations for weaker associations between BAI and vegetation indices using a global correlation include differences in species' inherent growth rates—the same amount of BAI can have different biological implications for productivity depending on a species' usual rate of

growth. There are also demonstrated cases where the relationship between a vegetation index and a particular biophysical property vary by species. For example, Fassnacht et al. (1997) found a much stronger association between NDVI and LAI as measured from the ground for conifers (r^2 ~0.7) than deciduous trees ($r^2 = 0.35$) due to NDVI saturating more quickly in deciduous forest. Both differences in growth rates and tree appearance in imagery may complicate a global relationship.

2.3.2. BAI and Vegetation Indices Correlation by Site

Comparing BAI to vegetation indices for each site 1984-2010 resulted in inconsistent associations overall. Of the 47 total sites, only 19 had significant ($p \leq 0.05$) relationships between any of the 55 vegetation indices and BAI measurements. After reducing the effective sample size to adjust for autocorrelation, only 10 sites still had significant relationships. Furthermore, there was no single vegetation index that was consistent across plots. NDVI, the most commonly used vegetation index in studies comparing tree-ring growth to remotely sensed imagery was significantly correlated to measurements of BAI at none of the 47 individual sites (mean $\rho = 0.009 \pm 0.236$, mean $p = 0.587 \pm 0.268$). The "best" index, as determined by being significantly correlated at the most sites with the most consistency was the middle infrared index (MIR), which was significantly correlated to BAI at five sites. MIR is calculated as Landsat TM band 5 / band 7 and was initially developed to identify mineral compounds in soils, but has been demonstrated to be related to the NIR/R simple ratio (which measures overall "greenness"), presumably due to its connection to leaf water content (Elvidge and Lyon 1985). The correlation between BAI and MIR at these five sites was relatively strong

(average $\rho = 0.609 \pm 0.078$). Among these sites with a significant relationship between BAI and MIR, there were not apparent similarities with regard to species composition (2 paper birch, 1 mixed hardwoods, 2 red spruce), sample size (from 10-17 years of data), average BAI (629 ± 366 mm), or geographic proximity. For an example of how BAI and vegetation indices appear plotted over the study period (1984-2010) from two example sites (one which had a significant relationship to MIR and one which did not) see Figure **4**.

In these site-by-site analyses, sample size (which is the number of years with both BAI and vegetation index data) was limited due to cloud cover masking Landsat data from certain sites as well as further penalization to account for temporal autocorrelation (17 of the sites had significant temporal autocorrelation in the vegetation index and/or BAI data) (

Table 1). The resulting average sample size for individual site analyses (10.78 ± 5.18) corresponds with notably low statistical power. Given these limitations, we also considered significance using a less conservative critical value (α) of 0.10. At this α level, 17 of the 47 sites had a significant relationship between BAI and at least one of the 55 vegetation indices. Again, however, there was no single vegetation index that had a significant relationship to BAI for all sites consistently.

Even using this less conservative critical value, no sites' BAI measurements 1984-2010 were significantly related to NDVI. Of the 55 vegetation indices compared, the vegetation index that was significantly correlated with BAI for the most sites in a logical direction (in this case directly) was the second normalized difference infrared index (NDII7). Measurements of NDII7 were significantly, positively correlated (which

one would expect) with BAI measurements at 7 sites (mean $\rho = 0.481 \pm .074$, mean $p = 0.063 \pm 0.023$). However, there were two sites that had a significant negative relationship (which one would not expect) between BAI and NDII7 as well (mean $\rho = -0.479 \pm .014$, mean $p = .0893 \pm 0.013$). NDII7 is a combination of the near infrared (band 4) and mid infrared (band 7) bands (Table 3) (Hunt and Rock 1989) and was developed to evaluate water content by utilizing the high water absorbance of band 7 (e.g., lower reflectance signals higher water content) and the cell structure information provided by band 4 (e.g., higher reflectance signals healthy intercellular air spaces).

It is interesting that the two vegetation indices (MIR, NDII7) that had a significant relationship to BAI measurements at the most sites are both associated with water levels in vegetation. This could be due to a range of different reasons including the direct association of water stress with reduced radial tree growth (Stahle et al. 2007, Klos et al. 2009) as well as water stress potentially serving as an indicator of the presence of other stressors such as insect and pathogen damage (Townsend et al. 2012). Being farther along the electromagnetic spectrum, the bands that compose these indices (band 4, 5, and 7) are less susceptible to atmospheric interference, which may also permit a stronger relationship between these vegetation indices and BAI to emerge.

Notably, comparisons of these two indices (MIR, NDII7) to estimates of actual water content field vegetation has had mixed results in other studies. MIR has been shown to be related to vegetation cover in the Southwest and (Elvidge and Lyon 1985) hypothesized this was due to this index being sensitive to water content, but this relationship has not been directly evaluated. Similarly, Hunt and Rock (1989) found that

using near-infrared and mid-infrared bands (e.g., NDII7) to monitor actual water levels for a variety of species only worked for very severe cases of water stress. The only field-based study we were able to identify used a simulated Landsat TM sensor mounted on a plane (Pierce et al. 1990) and found the strength of the relationship between the normalized difference infrared index using band 5 in place of band 7 (e.g., NDII5) and field measurements of water pressure varied based on the time of day. The sensor was able to see significant differences between healthy and severely girdled trees in the morning, but in afternoon imagery, no significant difference was visible between stands due to transpiration. Landsat imagery is collected at around the same time of day—approximately solar noon—a point in the day when the differences between normal and water-stressed trees was not still distinguishable in the Pierce et al. (1990) study.

Within-site analysis of the relationship between BAI and vegetation indices should hold constant factors such as species composition, topography, and soil properties that likely contribute variation in that relationship at a broader landscape scale. The fact that relatively few (21% using $\alpha = 0.05$; 36% using $\alpha = 0.10$) of these sites had a significant relationship between BAI and any of the 55 vegetation indices, and that no one index was significantly correlated with BAI at more than 7 sites suggests that there is not a consistent measurable relationship between BAI and any single vegetation index derived from Landsat 5 TM imagery. Having a limited number of years of Landsat imagery due to cloud cover and haze, compounded by the lack of imagery prior to 1984 likely reduced our power to see this relationship. To find significant correlations similar to those found in our global assessment ($\rho \sim 0.2$) at $\alpha = 0.05$ with power = 0.95 would

require 53 observations (online power calculator accessed from http://www.danielsoper.com/statcalc3/calc.aspx?id=9). Therefore, while the site by site assessment is the most conservative and statistically sound approach to these analyses, site by site comparisons are much more likely to miss potentially significant relationships.

2.3.3. Multi-Index Predictive Modeling

As the production of tree-rings is a complex process (Speer 2010), it is possible that a combination of multiple vegetation indices measuring different canopy characteristics may better predict BAI then any single vegetation index alone. To combine multiple vegetation indices into a single predictive equation, a stepwise linear regression was used to identify the best overall model. Using all data points, regardless of species type or year, the resulting four-term model included the raw Landsat band 3 value (red) and three hyperspectral indices adapted to Landsat band structure—the simple ratio pigment index (Peñuelas et al. 1993), the modified simple ratio (MSR 705) (Sims and Gamon 2002), and a combination of bands 2 and 4 (BNa)(Buschmann and Nagel 1993). Each of these indices was developed to measure different aspect of vegetation condition: the red portion of the spectrum (band 3) can indicate chlorophyll content and absorbance, SRPI measures the ratio of chlorophyll to carotenoids, MSR705 indicates overall "greenness," and BNa is designed to measure chlorophyll content. There was low autocorrelation between variables (maximum model variance inflation factor = 9.19). While this model (Figure 5) was highly statistically significant ($p = < 0.0001$), the low model fit ($r^2 = 0.120$, adjusted $r^2 = 0.115$) and high root mean square error (648.38

mm^2 compared to a mean BAI of 1013.57 mm^2) suggests that it may not be a very useful model from a predictive standpoint.

From visual inspection of the model, it also appears that data points are highly clustered by species type, further suggesting that there may be within-species differences in the relationship between BAI and remotely sensed metrics of forest condition. Comparing this model's residual values, grouped by species type, using an analysis of variance also showed significant ($p < 0.001$, $F = 58.07$) differences among species types (Figure 6). Similar to the findings from the previous analysis, this suggests that attempting to predict BAI from vegetation indices derived from Landsat imagery using a single landscape-wide predictive equation will not be as accurate as one that is species-specific.

Repeating the same stepwise linear regression analysis, but for each species type (Figure 7a-e) was limited by the smaller number of sites for some types (pine-4, mixed hardwoods-5, and mixed fir-spruce-birch-4). Using only the data collected by Halman et al. (2011) from paper birch trees at twelve sites in the Green Mountains of Vermont (Figure **7**a), model fit was much stronger ($p = <0.0001$, $r^2 = 0.302$, adj. $r^2 = 0.285$; RMSE = 224.73 with mean BAI = 553.60). The stepwise model fitting process retained the following vegetation indices for the final predictive equation: a modified derivative between bands 7 and 5 (FD75)(Pontius et al. 2005), the reflectance absorbance index (RAI), the greenness condition index (GI) (Sivanpillai et al. 2006), and the hyperspectral adapted to multispectral index (HAM) (Pontius in Review). These indices are designed to

measure canopy moisture content, leaf stress, vegetation biomass, and an integrated measure of "forest decline," respectively.

Potential reasons for relatively better modeling success for paper birch include a larger sample size: 12 sites fell into this species type and on average these sites had 19 (± 2.79) years of imagery data available, due in part to all sites falling in both Landsat row 29 / path 14 and row 29/ path 13. The dendrochronological sampling used to collect the tree-ring data was also specifically designed to capture a range of canopy conditions and elevation types, and included many declining trees that were in poor enough condition to have locally absent rings (Halman et al. 2011). By including a broader range of potential growth conditions, relationships between vegetation indices and BAI are more robust. Another potential explanation for the stronger predictive ability of this model compared to the model including all species, is that paper birch do not retain their photosynthetic material from one year to the next, thus reducing complications from a lagged radial growth response related to damaged needles retained from previous years. Lastly, these sites were also relatively close to one another (<50km apart), which means that they may be more likely to share characteristics not accounted for in the modeling process, that nevertheless likely affect BAI including precipitation patterns, storm and winter injury damage, and some soil properties.

The other species type with a large sample size available on which to base a predictive BAI model was red spruce (with 22 sites). Unlike the model developed for paper birch, however, this model (Figure 7b) performed more poorly than the global model ($p = <0.0001$, $r^2 = 0.116$, adjusted $r^2 = 0.107$, RMSE = 548.79 with mean BAI =

1048.65). The stepwise model fitting process retained the following vegetation indices for the final predictive equation for red spruce: the first derivative of two mid-infrared bands (Landsat band 7 and band 5) (FD75)(Pontius et al. 2005), optimized soil adjusted vegetation index (OSAVI) (Rondeaux et al. 1996), and the VogB index (Vogelmann et al. 1993). These indices are designed to measure canopy moisture content, total vegetation density adjusted for soil reflectance, and total chlorophyll content, respectively. Given this model's poor fit and high root mean square error relative to the average BAI measurement of these red spruce sites, it appears there is only a very weak relationship between BAI and vegetation indices derived from Landsat imagery—one that is probably too weak to be very ecologically meaningful.

Potential reasons for the poorer fit of this model include the fact that red spruce is often rarer (particularly at lower elevations) and has smaller crown size than deciduous species, making it is possible that other un-cored tree species contributed to the spectral information captured by Landsat. This would weaken the relationship between BAI and vegetation indices because the BAI measurements of red spruce may not be representative of growth of other species, which the sensor is also detecting. Like the birch sites cored by Halman et al. (2011), the majority of the red spruce sites (19 of 22) were also located to capture a range of elevation and canopy damage levels (Kosiba et al. in review). However, the red spruce sites were also distributed over a much larger portion of the landscape, across Vermont and New Hampshire, up to 130km apart. Thus these sites are less likely to experience similar climate and stress events that also contribute to tree-ring width that were not accounted for in the model. More red spruce

sites also had significant temporal autocorrelation in BAI measurements (34% compared to only 25% for paper birch sites), likely due in part to needle retention from year-to-year. This temporal autocorrelation in growth may contribute to the disconnect between BAI measurements and Landsat vegetation index measurements from the same year.

Because of the independent calibration and spectral difference inherent between species key model variables were not consistent across species. This further indicates that there is no "one" vegetation index that is able to capture BAI across the landscape.

2.3.4. Limitations and Next Steps

Our finding that there is not an observable, strong, consistent relationship between BAI and vegetation indices over a 27 year period is in contrast to many of the other studies that have analyzed tree-ring increment and remotely sensed metrics of forest condition. The majority of published studies on this topic have found moderate ($r = 0.366\text{-}0.59$; $r^2 = 0.44\text{-}0.59$, $p < 0.005$) (Malmström et al. 1997, D'Arrigo et al. 2000, Lopatin et al. 2006, Berner et al. 2011) to extremely strong ($r^2 = 0.91$, $p < 0.005$) (Kaufmann et al. 2004, Wang et al. 2004) associations between NDVI and tree-ring increment, even using data with much coarser spatial resolution (30m for Landsat vs. >8km for these other studies).

One potential reason for these stronger observed relationships is that the majority of sites used were located in boreal forests, which tend to be more homogeneous both in species composition and land use type. In contrast, forests in the Northeast typically have higher species diversity and patchier composition, which may make it more likely that trees of different species type and health conditions are being averaged

together spectrally in the imagery. With a longer and wetter growing season, forests in the Northeast also tend to experience catastrophic disturbance with less frequency than other forested ecosystems (Seymour et al. 2002). Less dramatic loss of canopy from disturbance events and relatively quick regeneration of the understory post-disturbance may also hamper the ability of Landsat imagery to "see" areas where trees have been damaged. This is because the sensor cannot detect the difference between older recovering vegetation and new vegetation that has grown in and taken its place. Furthermore, due to permitting restrictions and time constraints, only a subsample of trees were cored on each site. It is possible that the trees selected for coring were not fully representative of all the trees that contributed to a pixel's spectral response, due either to there being too few samples taken or non-representative trees being cored. The spectral response of the understory, which was not sampled, may also be contributing to the Landsat measurement (Spanner et al. 1990, Ghitter et al. 1995), particularly in places with sparser canopies such as the pine plantations cored in this study.

This study also had several temporal limitations that should be noted. Due to availability and processing requirements, yearly images used to calculate the vegetation indices were from a single date, whereas a tree-ring represents an integrated metric of forest condition over an entire year (and in some cases, previous years). Early growing season imagery may reflect growing conditions in the prior year, as initial leaf out is in part fueled by starch reserves (SOURCE). Imagery from earlier in the growing season may also not capture reduced growth rates that result from stress events later in the growing season such as drought or insect defoliation. Some studies have also found that

tree-rings correlate better with NDVI measurements from certain parts of the year, some of which were not in our June 10 -August 20 growing season definition. For example, in their study of an oak stand in Kansas, Wang et al. (2004) found that tree-rings correlated strongly with NDVI averaged over mid-May to June (r^2 =0.91), but only moderately well with the average (r^2 =0.76) or maximum (r^2 =0.25) NDVI value over a growing season (April-October). Kauffman et al. (2008) compared tree-ring data to NDVI at 53 deciduous sites south of 40ºN 1981-2003, and found that there was a positive correlation to NDVI in the months of April and May, no relationship June-September, and a negative relationship with October values. Interestingly, when repeating the same analysis on 48 deciduous and coniferous sites north of 40ºN, they found a positive significant relationships between tree-ring index and NDVI from June and July, and a negative one with May NDVI measurements. They speculate that this may be due to the effect climate has on both leaf development as well as tree-ring production. These findings suggest that using imagery from a single date for each year to calculate vegetation indices may have missed crucial portions of the growing season. However, given the expertise, time, and storage requirements involved with processing Landsat imagery, using multiple images from each year may not be feasible for many researchers.

Another potential temporal limitation of our study is that trees cored in 2006 (Halman), 2010 (Kosiba) and 2011 (Weverka) are not necessarily representative of the trees in that Landsat pixel over the entire study period 1984-2010. For example, at one site it is likely that several trees were harvested at some point between 2003 and 2010 (Kosiba, personal communication). In theory the Landsat sensor should have been able to

pick up that loss of biomass. The remaining trees at that site cored in 2010, however, would not have had any sign of reduced growth post- harvesting activity in their tree-ring records, and in fact may have experienced release. This difference between Landsat measurement of forest condition and the record contained in the tree-rings of individuals cored could lead to muddying of their relationship. In this particular example, this site was removed from this analysis to reduce that potential source of error. However, the history of many sites included in analysis remains unknown.

While there are many potential sources of error specific to this study, there is also some evidence that the relationship between canopy condition (which is what the Landsat imagery directly captures) and radial growth is somewhat complicated and non-linear. In a lengthy literature review on forest decline and basal area increment in Europe, Innes (1993) concluded that trees had to lose between 30% and 50% of their foliage before growth reductions were apparent in the tree-rings. There are similar examples of this in the Northeast where Schaberg et al. (2011) found examples of red spruce trees with 100% canopy loss that resulted in only a 60% reduction in radial growth for that year. Work by Smith and Shortle (2003) on hardwoods after the 1998 ice storm also revealed that for certain species (i.e., white ash), the degree of damage experienced appeared to have no effect on tree-ring increment immediately post-disturbance. There are also examples of the reverse of this phenomenon in the literature. Duchesne et al. (2003) found that reduction in ring-width preceded visual observations of decline at several of their sugar maple sites by at least a decade. Cherubini et al.(2002) and found

that in some cases tree-ring production stopped up to 30 years before a tree was considered dead based on visual observation of absence of foliage.

Another good example of this disconnect between foliage condition and radial growth can be drawn from several experiments carried out in the Hubbard Brook Experimental Forest in the White Mountains of New Hampshire. In this forest Wollastonite ($CaSiO_3$) was added to an experimental watershed in 1999 to mimic pre-industrial calcium levels. Post application, multiple studies found higher calcium levels and higher winter stress tolerance in red spruce trees in the experimental watershed versus the reference watershed (Hawley et al. 2006, Halman et al. 2008, Kessler 2008). There were also observable differences in spectral reflectance values from red spruce foliage from the two watersheds measured using a handheld spectroradiometer as well as Landsat 7 TM data (Kessler 2008). However, red spruce cored at four sites in the experimental watershed and four sites in the reference watershed in 2010 (which were also used in this analysis) appear to not have significantly divergent growth patterns since the application of calcium (Kosiba, personal communication). This example at Hubbard Brook, as well as the studies mentioned above illustrate a potential source of error in one of the crucial assumptions of this analysis—that canopy condition is strongly related to radial growth and can therefore serve as a link between the two metrics of forest condition (i.e., BAI and vegetation indices).

Given that there were only relatively weak relationships between BAI and any of the 55 vegetation indices considered, this raises the question about what biophysical properties of forest vegetation are driving the changes observed in vegetation indices.

Many of these vegetation indices used in this analysis have been developed in controlled lab settings or have been designed for hyperspectral sensors. Some previous attempts at evaluating the ecological basis of vegetation indices in the field have had poor results (Pierce et al. 1990).

However, Landsat imagery averages together reflectance values from all vegetation (and other ground cover) in a 30m x 30m pixel area, and thus may actually be providing a more comprehensive picture of biomass than what can be captured in the growth of 10-20 trees in the same pixel. For example, Wolter et al. (2008) were able to estimate basal area forest-wide with strong accuracy (r^2 = 0.62, RMSE 4.67m^2/ha. or 20% of measured basal area) using many of the same vegetation indices in our study derived from Landsat imagery from multiple seasons in Northern Minnesota and Ontario. Their accuracy rose considerably (r^2 = 0.65-0.88, RMSE = 4.99-12.32m^2/ha. or 16-23% of measured basal area) when calibrating their equation for individual species or forest types (i.e., deciduous, coniferous). In a study examining net primary productivity in the Bartlett Experimental Forest (where three sites used in our study were located), Potter et al. (2007) found a moderate relationship (r^2 = 0.50) between an NDVI-based model (with input data from 2001 Landsat imagery) and metrics of stand productivity (e.g., tree diameter, litter fall, and other factors derived from allometric equations) at 1900+ sites. Accounting for elevation and aspect further improved the model fit (r^2 = 0.69). These studies illustrate that remotely sensed imagery can be used to model forest productivity at a single point in time relatively well. It is possible that our findings in this study may be limited by attempting to see smaller scale changes (i.e., increment vs. total productivity)

as well as variability in the proportion of primary productivity (viewable by the Landsat sensor) that is ultimately allocated to radial trunk growth (tree-rings).

2.4. Conclusions

Statistically significant, although weak, relationships between BAI and some vegetation indices were observed. The most consistently significant indices across the three analyses (defined as either the strongest, or showing up in multiple analyses) include: NDII7, MIR, SARVI, OSAVI, Flo, SRPI, and VogB . These are designed to measure water stress, "greenness" (a combination of biomass, leaf area index, vegetation cover) adjusted for atmospheric and soil interference, and chlorophyll and carotenoid content. While NDVI is a very widely used vegetation index, in our analyses, it appears to have underperformed many other multispectral and hyperspectral indices. The strength of associations and model fit were also improved by focusing on single species types instead of attempting to carry out analyses on all sites, regardless of species composition.

These findings suggest that while remotely sensed products have been shown to be usable in identifying disturbance events (Rock et al. 1986, Vogelmann and Rock 1989, Cohen et al. 2002, Olthof et al. 2004, Townsend et al. 2012), factors such as the timing and availability of imagery, mixed pixel issues common to heterogeneous forests such as those in the Northeast, mortality and regeneration captured in pixels and not in cores, among other factors, may make it difficult to use this imagery to accurately model radial growth. If efforts were undertaken to model forest productivity (in terms of BAI) from Landsat imagery at the landscape scale, we suggest expanding the range of vegetation

indices beyond NDVI alone and developing species-specific equations as opposed to applying a single equation across an entire image. Any results should also be interpreted with care, understanding that accuracy may only be within 20-25% (proportion of RMSE/mean) of true BAI at best. While limited in absolute accuracy, in this study using a suite of vegetation indices derived from Landsat imagery to predict BAI was an improvement over NDVI alone and could potentially be used as a general relative measure of landscape scale productivity from year to year.

Tables:

Table 1: Data Summary by Site

Site ID	State	Collector	Species	#Trees	n (years w/ imagery and tree data)	n_{eff}	Significant relationship ($\alpha = 0.10$) between BAI and any VI's?
ABE042	VT	A. Weverka	ABBA BEPA PIRU	7 10 10	16	6	No
ABE043	VT	A. Weverka	ABBA BEAL	10 8	18	7	No
BAR001	NH	A. Weverka	PIRU	10	11	11	Yes
BAR002	NH	A. Weverka	FAGR	10	12	2	No
BAR003	NH	A. Weverka	PIRU	10	16	5	No
CAM070	VT	A. Weverka	ABBA PIRU	9 9	17	17	Yes
CAM071	VT	A. Weverka	ABBA BEPA PIRU	9 10 5	20	5	Yes
CEN001	VT	A. Weverka	PIST	10	20	20	Yes
CEN002	VT	A. Weverka	PIST	11	20	20	Yes
JRF229	VT	A. Weverka	PIRE	17	21	5	No
JRF242	VT	A. Weverka	PIRE	11	21	21	No
HEG018	NH	A. Weverka	PIRU	12	12	12	No
MIC001	NH	A. Weverka	ACSA BEAL FAGR	5 6 8	11	4	No
MIC002	VT	A. Weverka	ACSA BEAL FAGR	5 8 4	8	8	No
SUG001	VT	A. Weverka	ACRU FAGR	9 10	14	14	Yes
SUG002	VT	A. Weverka	ACSA BEAL FAGR	6 6 7	11	3	No
BKE58	VT	A. Kosiba	PIRU	10	13	13	No

BNT182	VT	A. Kosiba	PIRU	10	12	12	Yes
BNT185	VT	A. Kosiba	PIRU	10	10	10	Yes
CAR176	VT	A. Kosiba	PIRU	11	12	12	Yes
CAR180	VT	A. Kosiba	PIRU	10	11	11	Yes
HUB164	NH	A. Kosiba	PIRU	5	15	5	No
HUB165	NH	A. Kosiba	PIRU	5	15	6	No
HUB167	NH	A. Kosiba	PIRU	5	15	15	Yes
HUB168	NH	A. Kosiba	PIRU	5	15	15	No
HUB169	NH	A. Kosiba	PIRU	6	13	5	No
HUB171	NH	A. Kosiba	PIRU	6	13	4	No
HUB172	NH	A. Kosiba	PIRU	6	13	4	Yes
HUB174	NH	A. Kosiba	PIRU	6	13	5	No
MAN77	VT	A. Kosiba	PIRU	14	15	7	No
MID101	VT	A. Kosiba	PIRU	10	19	8	No
MOO158	NH	A. Kosiba	PIRU	10	15	15	No
MOO161	NH	A. Kosiba	PIRU	10	13	13	Yes
MRG127	VT	A. Kosiba	PIRU	10	18	18	No
MRG128	VT	A. Kosiba	PIRU	10	17	17	Yes
CH-Low	VT	J. Halman	BEPA	10	16	16	No
CH-Mid	VT	J. Halman	BEPA	20	15	15	No
CH-High	VT	J. Halman	BEPA	10	13	13	Yes
Granville	VT	J. Halman	BEPA	19	19	19	Yes
Roxbury	VT	J. Halman	BEPA	20	16	16	Yes
App. Gap	VT	J. Halman	BEPA	18	15	5	No
MHM-Low	VT	J. Halman	BEPA	10	12	12	No
MHM-Mid	VT	J. Halman	BEPA	19	10	10	Yes
MHM-High	VT	J. Halman	BEPA	7	11	11	No
MHW-Low	VT	J. Halman	BEPA	10	11	11	No
MHW-Mid	VT	J. Halman	BEPA	20	13	13	Yes
MHW-High	VT	J. Halman	BEPA	9	11	11	No

Species Code:

ABBA= *Abies balsamea* = balsam fir
ACRU = *Acer rubrum* = red maple
ACSA = *Acer sacharum* = sugar maple
BEPA =*Betula papyrifera* = paper birch
FAGR = *Fagus grandifola* = beech
BEAL =*Betula alleghensis* = yellow birch
PIST = *Pinus strobus* = white pine
PIRE = *Pinus resinosa* = red pine

Table 2: Landsat 5 TM Images Used

Landsat Scene (Row/Path)	**Date Images Obtained**
29/13 38 of 47 sites fell into this scene	8/3/1986, 7/5/1987, 6/21/1988, 7/26/1989, 7/13/1990, 7/16/1991, 6/16/1992, 8/16/1993, 7/8/1994, 7/29/1996, 6/30/1997, 7/3/1998, 7/28/2000, 7/14/2002, 7/1/2003, 7/3/2004, 8/7/2005, 7/9/2006, 6/26/2007, 6/12/2008, 8/18/2009, 6/18/2010 Missing Years: 1984, 1985, 1995, 2001
29/14 30 of 47 sites fell into this scene	8/14/1984, 7/22/1985, 7/25/1986, 8/13/1987, 7/30/1988, 8/10/1989, 8/8/1991, 6/13/1994, 8/5/1996, 7/26/1998, 6/11/1999, 7/2/2001, 7/21/2002, 6/6/2003, 7/26/2004, 6/27/2005, 7/16/2006, 8/4/2007, 7/15/2008, 7/27/2010, Missing Years: 1990, 1992, 1993, 1995, 1997, 2000, 2009

Table 3: Sources and equations for vegetation indices used

Vegetation Index	Landsat 5 TM band combination	Biophysical Parameter	Source	Expected relationship
NDVI	(B4-B3) / (B4 + B3)	"Greenness"	Rouse et al. 2004	+
AI	B3/B1	Foliar senescence	Wolter and Townsend 2011	-
DVI	B4-B3	"Greenness"	Jordan 1969	+
EVI	2.5*((B4-B3)/ B4)+ (6*B3) - (7.5*B1)+1))	"Greenness"	Huete et al. 2002	+
GI	B2/B3	Light Use Efficiency	Sivanpillai et al. 2006	+
MIR	B5/B7	leaf water content	Elvidge and Lyon 1985	+
MSAVI	0.5* (2*B4+1 –(Sqr((2*B4+1) *(2*B4-1))-(8*(B4-B3)))	"Greenness"	Qi et al. 1994	+
MSI	B5/B4	Moisture stress	Rock et al. 1986	-
NDII5	(B4-B5)/(B5-B4)	Leaf water content	Hardisky et al. 1983	+
NDII7	(B4-B7)/(B7-B4)	Leaf water content	Hunt and Rock 1989	+
OSAVI	(B4-B3) / (B4+B3+0.16)	Optimized "Greenness"	Rondeaux et al. 1996	+
RAI	B4/(B3+B5)	Leaf stress	Arzain and King 1997	-
RDVI	Sqr((B4-B3)/ ((B4+B3) *(B4-B3)))	"Greenness"	Roujean and Breon 1995	+

RVI	B4/B3	"Greenness"	Pearson and Miller 1972	+
SARVI	1.5* (B4-(B3-(B1-B3)) / (B4-(B3 + (B1-B3) + 0.5))	Soil-adjusted and atmosperhically resistant "Greenness"	Huete and Liu 1994	+
SAVI	1.5 *((B4-B3)/(B4+B3+0.5))	Soil-adjusted "Greenness"	Huete 1988	+
Aoki	B2/B4	chlorophyll content	Aoki et al. 1981	-
BNa	B3-B2	chlorophyll content	Buschman and Nagel 1993	-
CMS	B3/B4		Cater 1994	-
Datt	B3 *(B2*B3)	Total chlorophyll content	Datt 1998	
Dattb	B3/B2	$Chlorophyll_b$ content	Datt 1998	-
Flo	(B4-B2)/ (B5-B3)	chlorophyll fluorescence	Mohammed et al. 1995	+
Gitc	1/B3		Gitelson and Merzylac 2001	?
GM	B4/B2		Gitelson and Merzylac 1994	?
MCARI1	1.2 * ((2.5*B3)-1.3(B4-B2)))	green leaf area index	Haboudane et al. 2004	+
MCARI2	1.5 * ((2.5 *((B4-B3))- (1.3 *(B4-B2)))/ (Sqr(((2*B4+1) * (2*B4 +1))) – (6*B4-(5* Sqr(B3)))-0.5))	green leaf area index	Haboudane et al. 2004	+
MND705	(B4-B3)/ (B4+B3 +(2*B1))	Chlorophyll: carotenoids	Sims and Gamon 2002	-
MSR	((B4/B3-1) / (Sqr((B4/B3)+1))		Chen 1996	
MSR705	(B4-B1)/(B4+B1)	Chlorophyll: carotenoids	Sims and Gamon 2002	-
MTVI	1.2 *((1.2*(B4-B2))-(2.5*(B3-B2))	green leaf area index	Haboudane et al. 2004	+
MTVI2	1.2 *((1.2*(B4-B2))-(2.5*(B3-B2)) /(Sqr (((2*B4+1)*(2*B4+1)) – (6*B4 – (5* (Sqr(B3)))) – 0.5))	green leaf area index	Haboudane et al. 2004	+
NPCI	(B3-1)/(B3+B1)	Total pigments: $chlorophyll_a$	Penuelas et al. 1993	-
PSSRa	B4/B3		Blacburn 1998	+
SIPI	(B4-B1)/(B4+B3)	carotenoids: chlorophyll	Penuelas 1995	-
SRPI	B1/B3	carotenoids: chlorophyll	Penuerlas 1993	+
TVI	0.5 * (120 *(B4-B2) -200 *(B3-B2))		Broge and LeBlanc 2001	+
VogB	(B4-B3) / (B5-B4)	Chlorophyll content	Vogelmann et al. 1993	+

HAM	- 51.76 + (B5*0.946) + ((B2/B4) * 0.706) - ((1.5*((2.5*(B4-B3)) - (1.3*(B4- B2))) / (Sqrt((((2*B4+1) * (2*B4+1)))) - (6*B4 - (5*(Sqrt(B3))) 0.5))) *0.236) + ((B4-B1) / (B4-B3) *54.536) + ((B4-B2) / (B5 - B3) * 0.451)	Forest decline	Pontius et al. in review	-

Band	**Name**	**Wavelength**
Landsat 5 TM Band 1 (B1)	"blue"	0.45- 0.52 µm
Landsat 5 TM Band 2 (B2)	"green"	0.52- 0.60 µm
Landsat 5 TM Band 3 (B3)	"red"	0.63- 0.69 µm
Landsat 5 TM Band 4 (B4)	"near infrared"	0.76- 0.90 µm
Landsat 5 TM Band 5 (B5)	"short-wave infrared"	1.55- 1.75 µm
Landsat 5 TM Band 7 (B7)	"mid infrared"	2.08- 2.35 µm

Table 4: Vegetation Indices with a significant relationship to BAI, across all years and all sites

Vegetation Index	**Absorbance Feature**	**Spearman ρ**	**p-value**
NPCI	Total Pigments: chlorophyll $_a$	-0.1572	<.0001
SIPI	Chlorophyll: Carotenoids	-0.1555	<.0001
HAM	Forest Health	-0.138	0.0002
MSR705	Chlorophyll: Carotenoids	-0.107	0.0046
MND705	Chlorophyll: Carotenoids	-0.087	0.0214
MSI	Moisture Stress	-0.084	0.0238
B7	Moisture Stress	-0.0757	0.0418
B5	Moisture Stress	-0.0719	0.0497
SARVI	LAI, green biomass, absorbed photosynthetically active radiation	0.0773	0.0409
NDII7	Leaf Water Content	0.0819	0.0276
NDII5	Leaf Water Content	0.0838	0.0242
Flo	Chlorophyll Fluorescence	0.0935	0.0118
VogB	Chlorophyll Content	0.0935	0.0118
SRPI	Chlorophyll: Carotenoids	0.1505	<.0001

Table 5: Vegetation indices with a significant relationship to BAI by species type

Species Type	Vegetation Index	Spearman rho	p-value	Species Type	Vegetation Index	Spearman rho	p-value
Birch	SD34	-0.3535	<.0001	Mixed Hardwoods	MSI*	-0.3275	0.0088
Birch	SD43	-0.3535	<.0001	Mixed Hardwoods	NDII7*	0.2813	0.0255
Birch	MSI	-0.3505	<.0001	Mixed Hardwoods	RAI	0.2861	0.023
Birch	FD54	-0.3415	<.0001	Mixed Hardwoods	NDII5*	0.3275	0.0088
Birch	SIPI*	-0.3317	<.0001	Mixed Hardwoods	VogB*	0.3327	0.0077
Birch	SD4	-0.3114	<.0001	Mixed Hardwoods	Flo*	0.343	0.0059
Birch	HAM*	-0.3111	<.0001	Mixed Fir-Spruce-Birch	MCARI1	-0.5614	<.0001
Birch	MCARI1	-0.3075	<.0001	Mixed Fir-Spruce-Birch	SD4	-0.5448	<.0001
Birch	SARVI	-0.2737	0.0003	Mixed Fir-Spruce-Birch	SARVI*	-0.5379	<.0001
Birch	SD54	-0.2699	0.0002	Mixed Fir-Spruce-Birch	FD54	-0.5346	<.0001
Birch	TD720	-0.2681	0.0003	Mixed Fir-Spruce-Birch	SD34	-0.531	<.0001
Birch	NPCI	-0.2472	0.001	Mixed Fir-Spruce-Birch	SD43	-0.531	<.0001
Birch	FD75	-0.1818	0.014	Mixed Fir-Spruce-Birch	TD720	-0.522	<.0001
Birch	GM	0.16	0.031	Mixed Fir-Spruce-Birch	SD54	-0.5155	<.0001
Birch	MIR	0.2426	0.001	Mixed Fir-Spruce-Birch	FD75	-0.3556	0.0019
Birch	SRPI*	0.2591	0.0006	Mixed Fir-Spruce-Birch	MSI*	-0.2643	0.0229
Birch	B4	0.2744	0.0002	Mixed Fir-Spruce-Birch	B7*	0.2586	0.0261
Birch	MTVI2	0.2744	0.0002	Mixed Fir-Spruce-Birch	Flo*	0.2596	0.0255
Birch	MTVI	0.2775	0.0001	Mixed Fir-Spruce-Birch	VogB*	0.2643	0.0229
Birch	SD3	0.2787	0.0001	Mixed Fir-Spruce-Birch	NDII5*	0.2649	0.0226
Birch	TVI	0.2814	0.0001	Mixed Fir-Spruce-Birch	B5*	0.347	0.0025
Birch	DVI	0.2876	<.0001	Mixed Fir-Spruce-Birch	EVI	0.4811	<.0001
Birch	FD43	0.2876	<.0001	Mixed Fir-Spruce-Birch	B4	0.5234	<.0001
Birch	MSAVI	0.2876	<.0001	Mixed Fir-Spruce-Birch	SD3	0.5367	<.0001
Birch	BNa	0.2917	<.0001	Mixed Fir-Spruce-Birch	MTVI	0.5378	<.0001
Birch	RDVI	0.297	<.0001	Mixed Fir-Spruce-Birch	TVI	0.5394	<.0001
Birch	MCARI2	0.2976	<.0001	Mixed Fir-Spruce-Birch	BNa	0.5413	<.0001
Birch	SAVI	0.2984	<.0001	Mixed Fir-Spruce-Birch	DVI	0.5439	<.0001
Birch	RAI	0.2992	<.0001	Mixed Fir-Spruce-Birch	FD43	0.5439	<.0001
Birch	OSAVI	0.3003	<.0001	Mixed Fir-Spruce-Birch	MSAVI	0.5439	<.0001
Birch	EVI	0.3089	<.0001	Mixed Fir-Spruce-Birch	MTVI2	0.5455	<.0001
Birch	VogB*	0.3469	<.0001	Mixed Fir-Spruce-Birch	OSAVI	0.5498	<.0001
Birch	NDII5*	0.3508	<.0001	Mixed Fir-Spruce-Birch	MCARI2	0.5589	<.0001
Birch	Flo*	0.3609	<.0001	Mixed Fir-Spruce-Birch	SAVI	0.5625	<.0001
Birch	NDII7*	0.3663	<.0001	Mixed Fir-Spruce-Birch	RDVI	0.5635	<.0001

Species Type	Vegetation Index	Spearman rho	p-value
Pine	HAM*	-0.4308	<.0001
Pine	SIPI*	-0.4001	0.0001
Pine	MSR705*	-0.3846	0.0003
Pine	NPCI*	-0.3364	0.0016
Pine	MND705*	-0.3236	0.0025
Pine	FD75	-0.3119	0.0037
Pine	GM	-0.2548	0.0186
Pine	Gitc	-0.226	0.0375
Pine	B3	0.234	0.0311
Pine	B2	0.2419	0.0257
Pine	B5*	0.2704	0.0123
Pine	SRPI*	0.3463	0.0012

* = also significant ($p < 0.05$) in the global correlation index (Table 4)

Species Type	Vegetation Index	Spearman rho	p-value
Red Spruce	Flo*	-0.2258	<.0001
Red Spruce	VogB*	-0.2206	<.0001
Red Spruce	MCARI1	-0.1973	0.0004
Red Spruce	FD75	-0.1867	0.0008
Red Spruce	CS	-0.1758	0.0016
Red Spruce	SD54	-0.1753	0.0016
Red Spruce	SARVI	-0.1734	0.0022
Red Spruce	NDII5*	-0.1674	0.0027
Red Spruce	TD720	-0.1557	0.0052
Red Spruce	Aoki	-0.1482	0.0079
Red Spruce	HAM*	-0.1439	0.0112
Red Spruce	NDII7*	-0.1406	0.0118
Red Spruce	SD4	-0.1345	0.0161
Red Spruce	GM	0.141	0.0116
Red Spruce	MND705	0.1485	0.0088
Red Spruce	B4	0.1524	0.0063
Red Spruce	BNa	0.1635	0.0034
Red Spruce	SD3	0.1676	0.0026
Red Spruce	MSI*	0.1676	0.0026
Red Spruce	MTVI	0.168	0.0026
Red Spruce	TVI	0.1683	0.0025
Red Spruce	EVI	0.1686	0.0029
Red Spruce	DVI	0.1693	0.0024
Red Spruce	FD43	0.1693	0.0024
Red Spruce	MSAVI	0.1693	0.0024
Red Spruce	NDVI	0.1758	0.0016
Red Spruce	PSSRa	0.1762	0.0016
Red Spruce	RVI	0.1762	0.0016
Red Spruce	MSR	0.1779	0.0014
Red Spruce	SAVI	0.182	0.0011
Red Spruce	B7*	0.185	0.0009
Red Spruce	B5*	0.194	0.0005
Red Spruce	RDVI	0.1949	0.0005
Red Spruce	MCARI2	0.2013	0.0003
Red Spruce	OSAVI	0.2087	0.0002
Red Spruce	MTVI2	0.2142	0.0001

Figures:

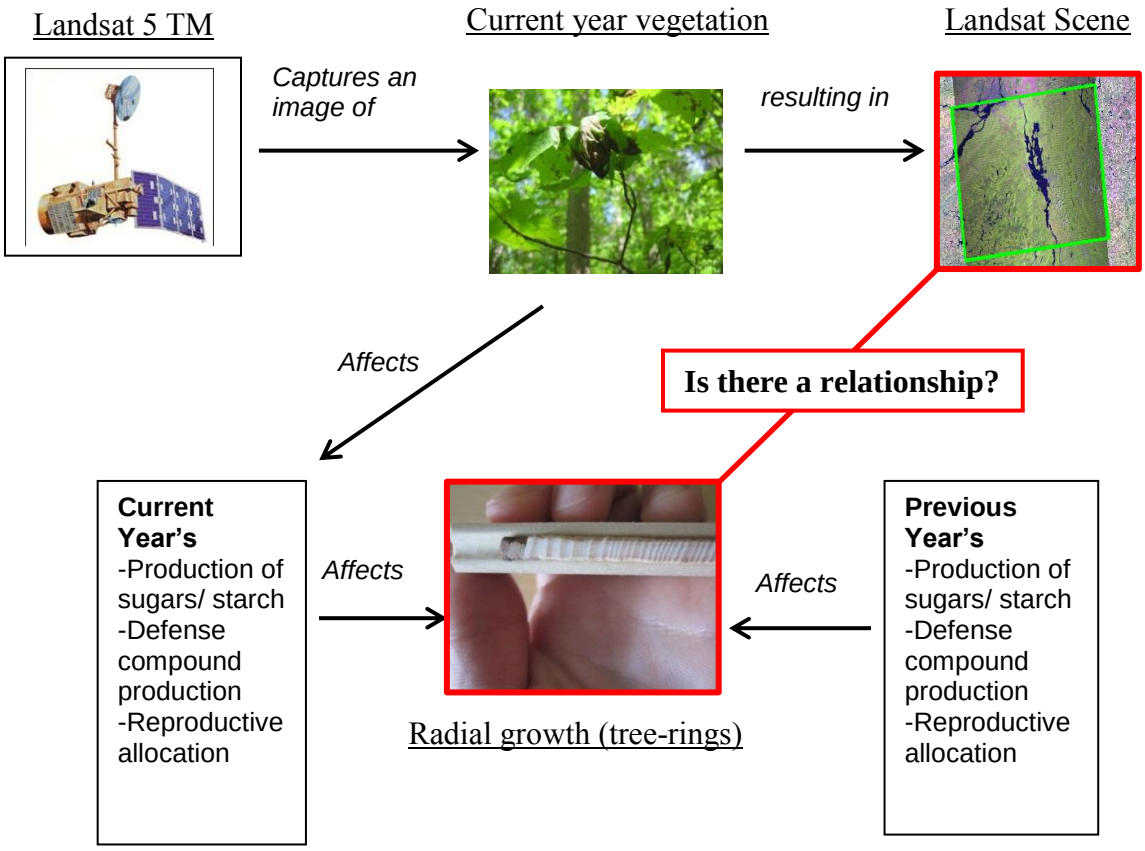

Figure 1: A conceptual model of the hypothesized relationship between Landsat imagery and radial-growth (tree-rings)

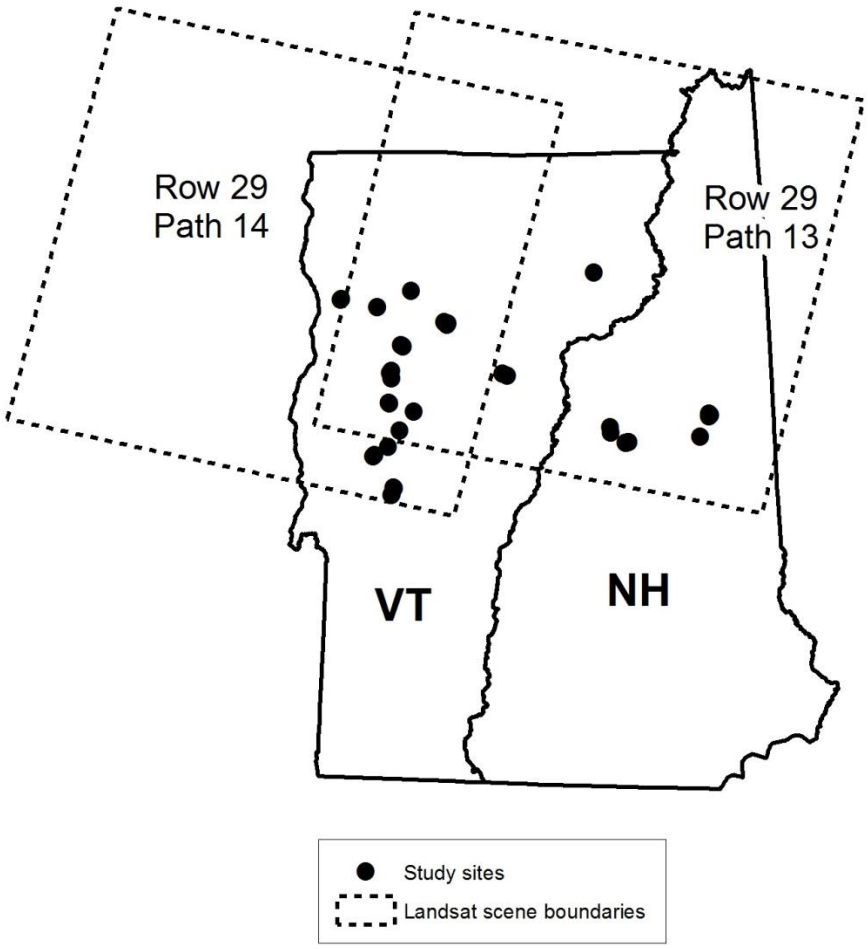

Figure 2: Map of the study region with Landsat 5 TM scene boundaries and site locations

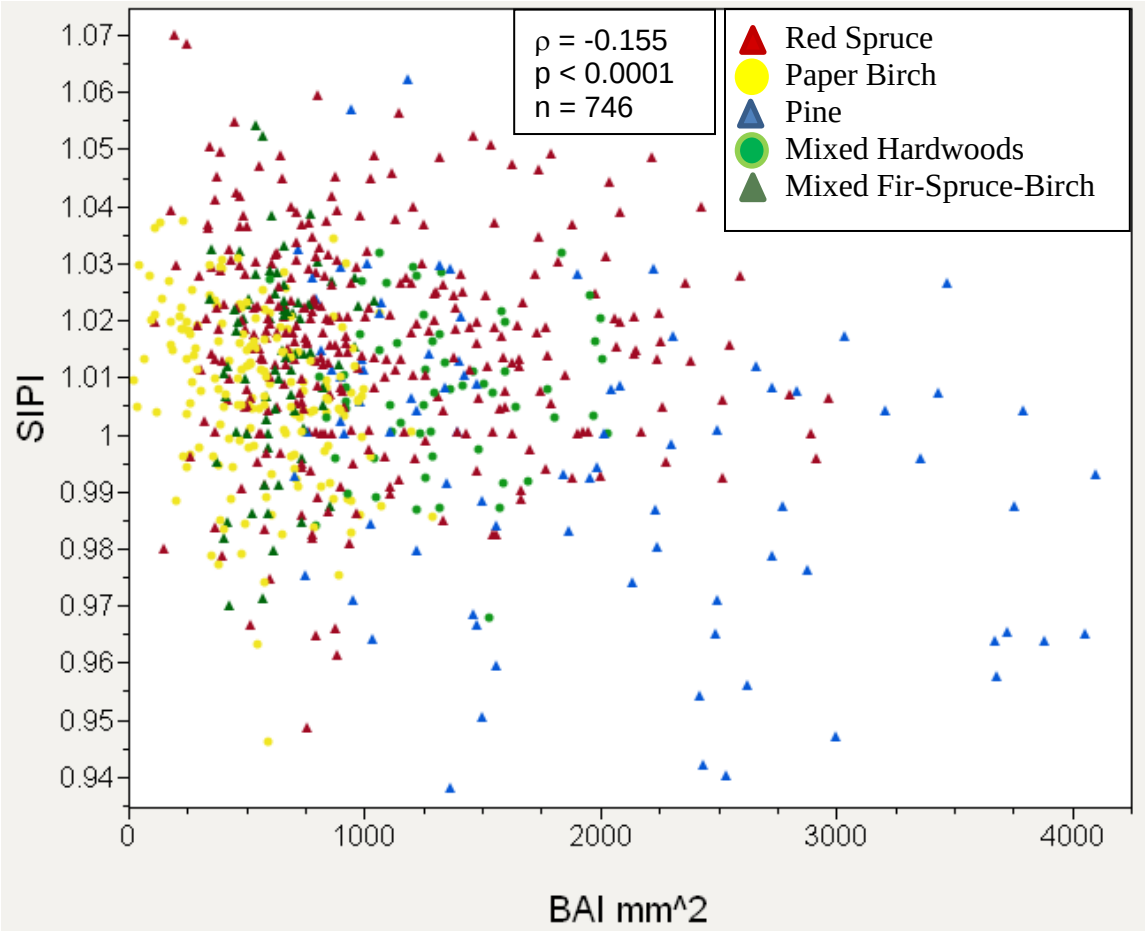

Figure 3: An example of the "global" (all years and all sites) relationship between BAI and vegetation index measurements, in this case the structure insensitive pigment index (SIPI)(Peñuelas et al. 1995). Data points are color coded by species. Note the obvious clustering of similar species types.

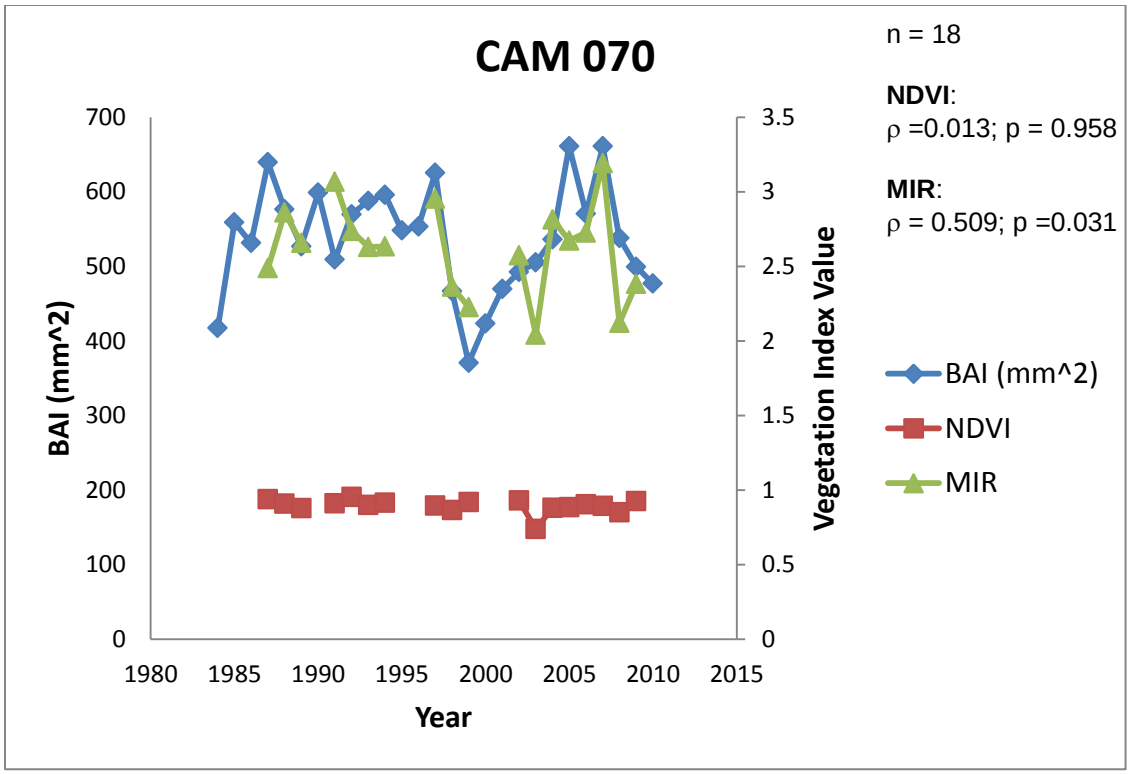

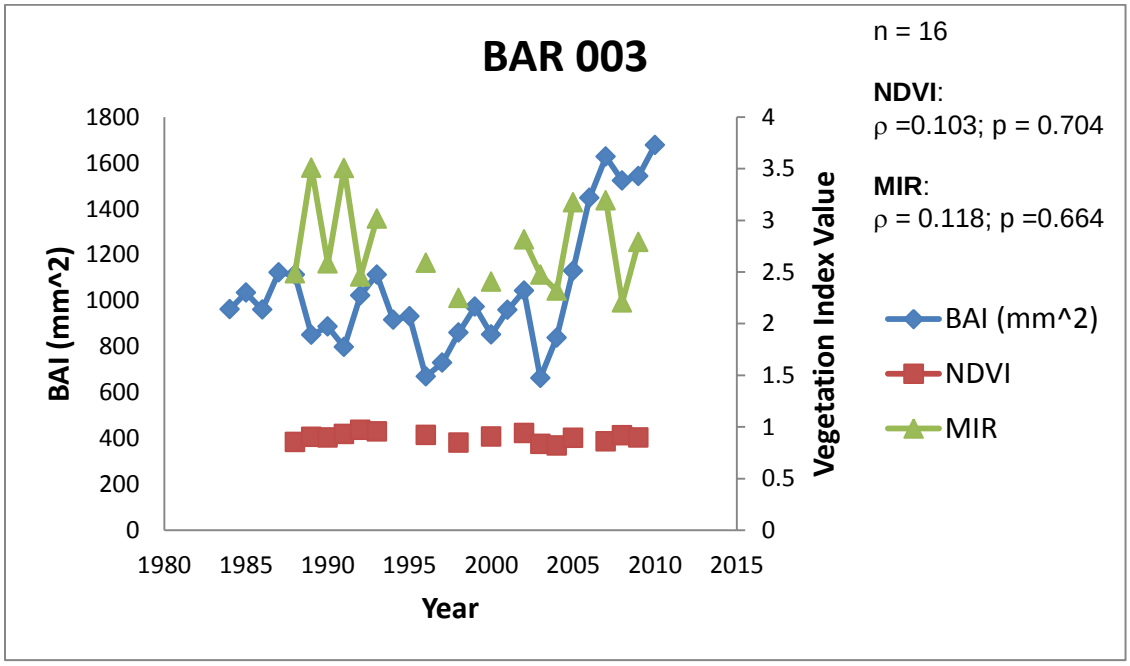

Figure 4: BAI vs. NDVI and MIR for two sites: CAM070 (with a significant relationship to MIR) and BAR003 (without a significant relationship to MIR). Gaps in the vegetation index values are years where imagery was not available.

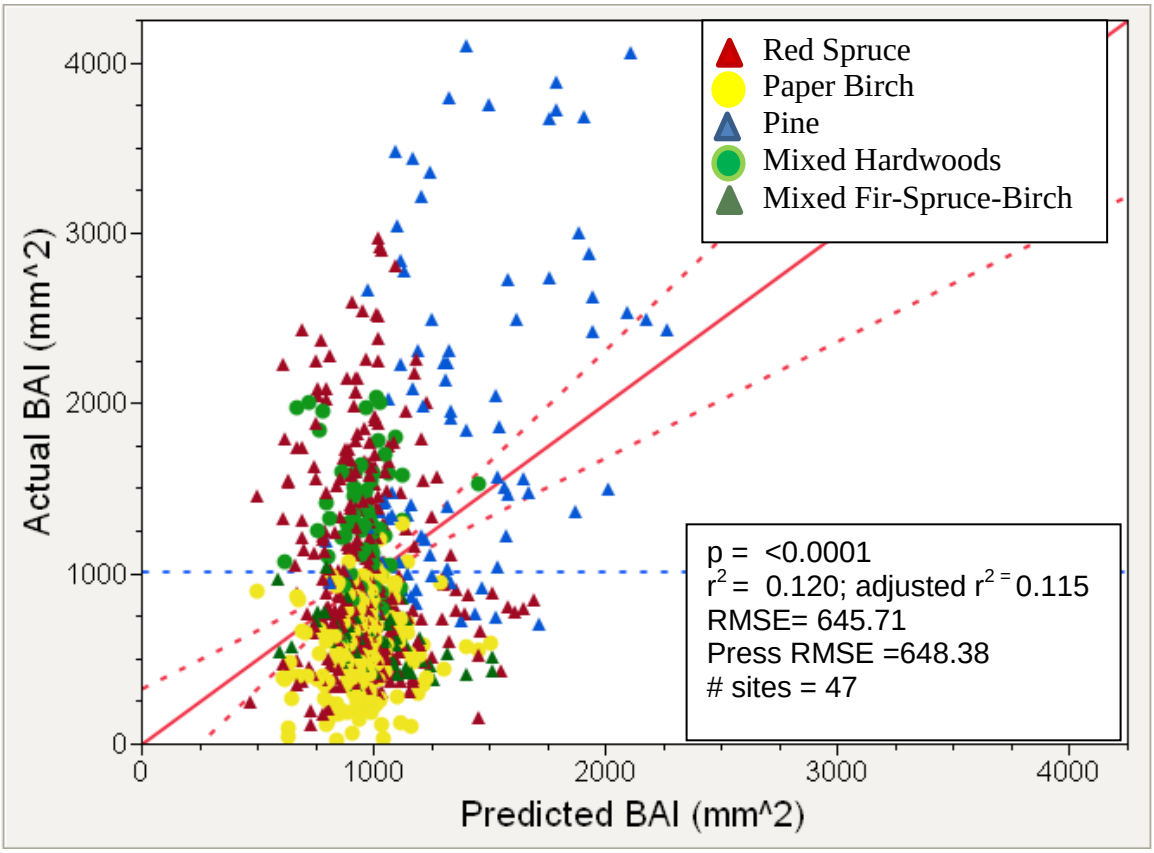

Figure 5: The four-term model that predicts BAI (mm^2) with r^2 = 0.120, RMSE = 645.71 using the following equation developed with data points from all species types and all years: 12148.476 - 61358.22* (***B3***) + 1714.863*(***BNa***) -11198.23*(***MSR705***) - 541.938*(***SRPI***).

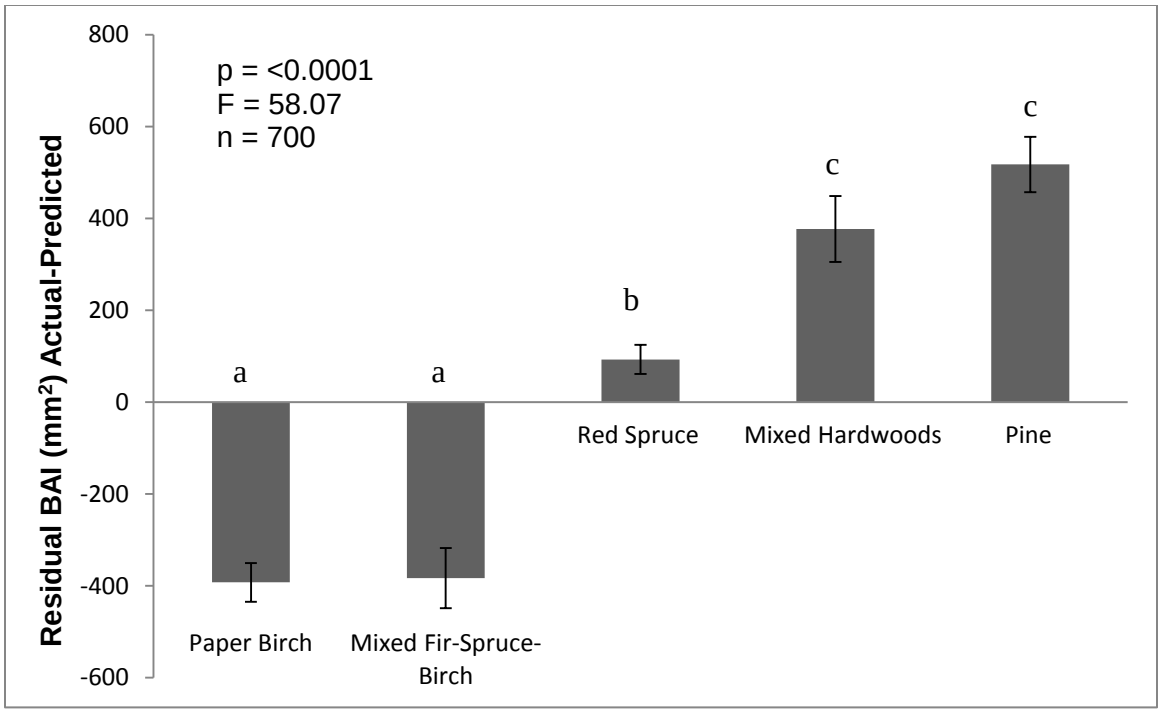

Figure 6: Average residual values from the global model predicting BAI from Band 3, SRPI, MSR705 and BNa (Fig. 5) by species type. Values are mean ± 1 S.E. Means with different letters differ significantly (F =58.07, p = <0.0001, n = 700).

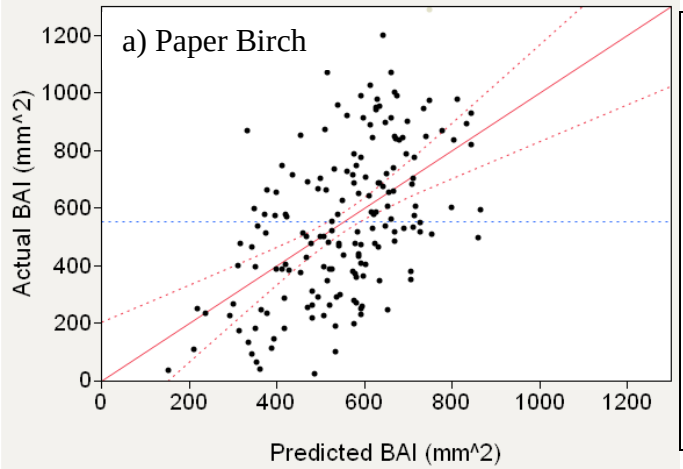

p = <0.0001
r^2 = 0.302; adjusted r^2 = 0.285
RMSE= 224.73
Press RMSE =227.37
sites = 12

Equation:
BAI (mm^2) =
*168.573 - (**FD75***2141.902) - (**GI***218.683) + (**RAI***456.432) - (**HAM***199.696)*

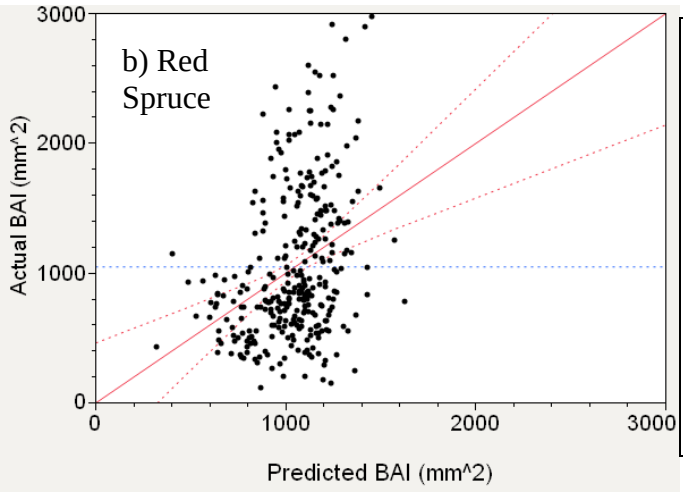

p = <0.0001
r^2 = 0.116; adjusted r^2 = 0.107
RMSE= 548.79
Press RMSE = 551.87
sites = 22

Equation:
BAI (mm^2) =
*-2664.277 + (**FD75***9336.504) + (**OSAVI***4347.924) + (**VogB***1146.568)*

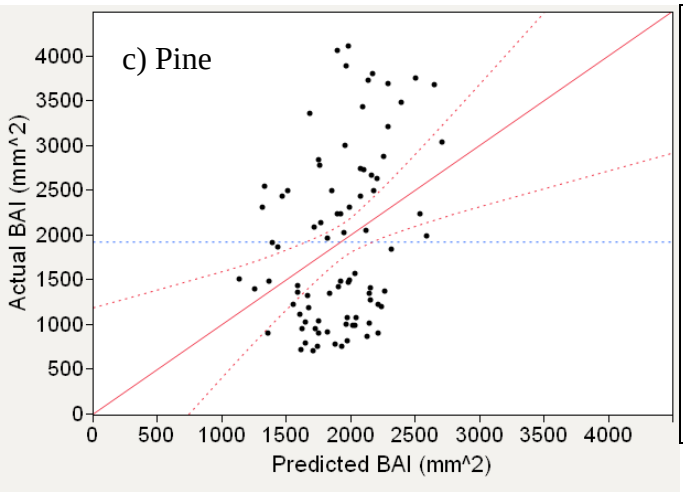

p = 0.0016
r^2 = 0.114 ; adjusted r^2 = 0.103
RMSE= 911.2357
Press RMSE = 919.582
sites = 4

Equation:
BAI (mm^2) =
*14.872- (**FD75***42301.793)*

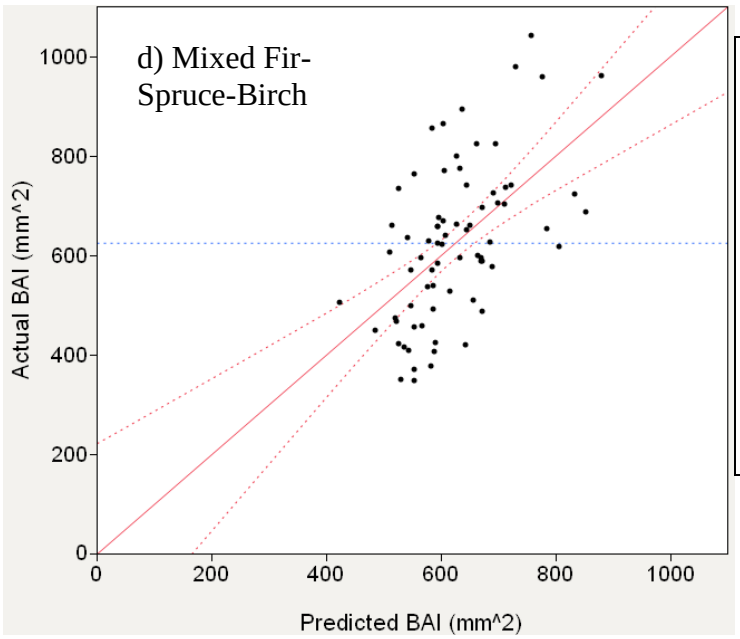

p = <0.0001
r^2 = 0.311; adjusted r^2 = 0.301
RMSE=131.571
Press RMSE = 133.64655
sites = 4

Equation:
BAI (mm^2) =
*-213.725 + (**SAVI***1818.632)*

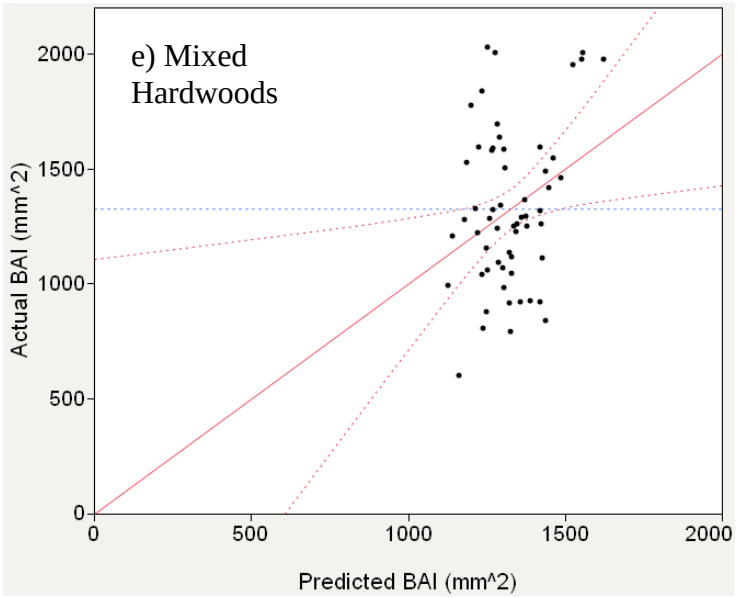

p = 0.0194
r^2 = 0.094; adjusted r^2 = 0.077
RMSE= 332.64
Press RMSE = 339.81
sites = 5

Equation:
BAI (mm^2) =
*1016.202 - (**SARVI***104.291)*

Figure 7: Actual vs. predictive BAI models developed using stepwise model fitting for the following species types: a) Paper Birch, b) Red Spruce c) Pine d) Mixed Fir-Spruce-Birch e) Mixed Hardwoods.

Appendix A:

R code developed by A. Bunn (used in Berner et al. 2011) to calculate the effective sample size of a dataset relative to its degree of temporal autocorrelation. This code is adapted from work by Dawdy and Matalas (1964).

```
# this calculates neff between x and y
calc.neff <- function(x,y){
  x.ar1 = acf(x,plot=F)
  sig.lvl = qnorm((1 + 0.95)/2)/sqrt(x.ar1$n.used)
  x.ar1 = x.ar1$acf[2,1,1]
  x.ar1 = ifelse(x.ar1 < sig.lvl, 0, x.ar1)

  y.ar1 = acf(y,plot=F)
  sig.lvl = qnorm((1 + 0.95)/2)/sqrt(y.ar1$n.used)
  y.ar1 = y.ar1$acf[2,1,1]
  y.ar1 = ifelse(y.ar1 < sig.lvl, 0, y.ar1)

  n <- length(x)
  neff <- floor(n*(1-x.ar1*y.ar1)/(1+x.ar1*y.ar1))
  neff
}
# on a df does each column
calc.neff2 <- function(dat){
  dat.acf <- rep(NA,ncol(dat))
  for(i in 1:ncol(dat)){
    tmp = acf(dat[,i],plot=F)
    sig.lvl = qnorm((1 + 0.95)/2)/sqrt(tmp$n.used)
    tmp2 = tmp$acf[2,1,1]
    dat.acf[i] = ifelse(tmp2 < sig.lvl, 0, tmp2)
  }
  dat.acf2 <- data.frame(x = dat.acf[1], y = dat.acf[-1])
  n <- nrow(dat)
  neff <- floor(n*(1-dat.acf2$x*dat.acf2$y)/(1+dat.acf2$x*dat.acf2$y))
  neff
}
```

Literature Cited:

Allen, C. D. 2009. Climate-induced forest dieback: An escalating global phenomenon? Unsylva **60**:43-39.

Babst, F., J. Esper, and E. Parlow. 2010. Landsat TM/ETM+ and tree-ring based assessment of spatiotemporal patterns of the autumnal moth (Epirrita autumnata) in northernmost Fennoscandia. Remote Sensing of Environment **114**:637-646.

Bauer, G., E.-D. Schulze, and M. Mund. 1997. Nutrient contents and concentration in relation to growth of *Picea abies* and *Fagus sylvatica* along a European transect. Tree Physiology **17**:777-786.

Berner, L. T., P. S. A. Beck, A. G. Bunn, A. H. Lloyd, and S. J. Goetz. 2011. High-latitude tree growth and satellite vegetation indices: Correlations and trends in Russia and Canada (1982-2008). J. Geophys. Res. **116**:G01015.

Biondi, F. 1999. Comparing tree-ring chronologies and repeated timber inventories as forest monitoring tools. Ecological Applications **9**:216–227.

Buschmann, C. and E. Nagel. 1993. In vivo spectroscopy and internal optics of leaves as basis for remote sensing of vegetation. International Journal of Remote Sensing **14**:711-722.

Canada Centre for Remote Sensing. 2007. Fundamentals of Remote Sensing. Canada Centre for Remote Sensing.

Chander, G., B. L. Markham, and D. L. Hedler. 2009. Summary of current radiometric calibration coefficients for Landsat MSS, TM, ETM+, and EO-1 ALI sensors. Remote Sensing of Environment **113**:893-903.

Cherubini, P., G. Fontana, D. Rigling, M. Dobbertin, P. Brang, and J. L. Innes. 2002. Tree-life histories prior to death: two fungal root pathogens affect tree-ring growth differently Journal of Ecology **90**:839-850.

Cohen, W. B. and S. N. Goward. 2004. Landsat's Role in Ecological Applications of Remote Sensing. BioScience **54**:535-545.

Cohen, W. B., T. A. Spies, R. J. Alig, D. R. Oetter, T. K. Maiersperger, and M. Fiorella. 2002. Characterizing 23 Years (1972–95) of Stand Replacement Disturbance in Western Oregon Forests with Landsat Imagery. Ecosystems **5**:122-137.

Cook, E. R., A. H. Johnston, and T. J. Blasing. 1987. Forest decline: modeling the effect of climate in tree rings. Tree Physiology **3**:27-40.

Cunningham, S. C., R. M. Nally, J. Read, P. J. Barker, M. White, J. R. Thomson, and P. Griffioen. 2009. A robust technique for mapping vegetation condition across a major river system. Ecosystems **12**:207-219.

D'Arrigo, R., R. Wilson, B. Liepert, and P. Cherubini. 2008. On the 'Divergence Problem' in Northern Forests: A review of the tree-ring evidence and possible causes. Global and Planetary Change **60**:289-305.

D'Arrigo, R. D., C. M. Malmstrom, G. C. Jacoby, S. O. Los, and D. E. Bunker. 2000. Correlation between maximum density of annual tree rings and NDVI based estimates of forest productivity. International Journal of Remote Sensing **21**:2239-2336.

Dale, V. H., L. A. Joyce, S. McNutly, R. P. Neilson, M. P. Ayres, M. D. Flanagan, P. J. Hanson, L. C. Irland, A. E. Lugo, C. J. Peterson, D. Simberloff, F. Swanson., B. J. Stocks, and B. M. Wotton. 2001. Climate Change and Forest Disturbances. BioScience **51**:723-734.

Datt, B. 1998. Remote Sensing of Chlorophyll a, Chlorophyll b, Chlorophyll a+b, and Total Carotenoid Content in Eucalyptus Leaves. Remote Sensing of Environment **66**:111-121.

Dawdy, D. R. and N. C. Matalas. 1964. Analysis of variance, covariance, and time series.*in* V. T. Chow, editor. Handbook of applied hydrology. McGraw-Hill New York, NY.

Driscoll, C. T., G. B. Lawrence, A. J. Bulger, T. J. Butler, C. S. Cronan, C. Eagar, K. F. Lambert, G. E. Likens, J. L. Stoddard, and K. C. Weathers. 2001. Acidic deposition in the Northeastern United States: Sources and inputs , ecosystem effects, and management strategies. BioScience **51**:180-198.

Duchesne, L., R. Ouimet, and C. Morneau. 2003. Assessment of sugar maple health based on basal area growth pattern. Canadian Journal of Forest Research **33**:2074-2080.

Dukes, J. S., J. Pontius, D. Orwig, J. R. Garnas, V. L. Rodgers, N. Brazee, B. Cooke, K. A. Theoharides, E. E. Stange, R. Harrington, J. Ehrenfeld, J. Gurevitch, M. Lerdau, K. Stinson, R. Wick, and M. Ayres. 2009. Responses of insect pests, pathogens, and invasive plant species to climate change in the forests of northeastern North America: What can we predict? Canadian Journal of Forest Research **39**:231-248.

Elvidge, C. D. and R. J. P. Lyon. 1985. Estimation of the Vegetation Contribution to the 1.65/2.22-Mu-M Ratio in Airborne Thematic-Mapper Imagery of the Virginia Range, Nevada. International Journal of Remote Sensing **6**:75-88.

Environmental Protection Agency. 2010. Inventory Of U.S. Greenhouse Gas Emissions and Sinks: 1990-2008. 430-R-10-006.

Ferretti, M. 1997. Forest health assessment and monitoring--issues for consideration. Environmental Monitoring and Assessment **48**:45-72.

Forbes, B. C., M. M. Fauria, and P. Zetterberg. 2009. Russian Arctic warming and 'greening' are closely tracked by tundra shrub willows. Global Change Biology **16**:1542-1554.

Franklin, S. E., M. A. Wulder, R. S. Skakun, and A. L. Carroll. 2003. Mountain Pine Beetle Red-Attack Forest Damage Classification Using Stratified Landsat TM Data in British Columbia, Canada. Photogrammetric Engineering and Remote Sensing **69**:283-288.

Ghitter, G. S., R. J. Hall, and S. E. Franklin. 1995. Variability of Landsat Thematic Mapper data in boreal deciduous and mixed-wood stands with conifer understory. International Journal of Remote Sensing **16**:2989-3002.

Goodale, C. L., M. J. Apps, R. A. Birdsey, C. B. Field, L. S. Heath, R. A. Houghton, J. C. Jenkins, G. H. Kohlmaier, W. Kurz, S. Liu, G.-J. Nabuurs, S. Nilsson, and A. Z. Shvidenko. 2002. Forest Carbon Sinks in the Northern Hemisphere. Ecological Applications **12**:891-899.

Grissino-Mayer, H. D. 2001. Evaluating crossdating accuracy: A manual and tutorial for the computer program COFECHA. Tree-ring Research **57**:205-221.

Halman, J. M., P. G. Schaberg, G. J. Hawley, and C. Eagar. 2008. Calcium addition at the Hubbard Brook Experimental Forest increases sugar storage, antioxidant activity and cold tolerance in native red spruce (Picea rubens). Tree Physiology **28**:855-862.

Halman, J. M., P. G. Schaberg, G. J. Hawley, and C. F. Hansen. 2011. Potential role of soil calcium in recovery of paper birch following ice storm injury in Vermont, USA. Forest Ecology and Management **261**:1539-1545.

Hawley, G. J., P. G. Schaberg, C. Eagar, and C. H. Borer. 2006. Calcium addition at the Hubbard Brook Experimental Forests reduced winter injury to red spruce in a high-injury year. Canadian Journal of Forest Research **36**:2544-2549.

Hornbeck, J. W. and R. B. Smith. 1985. Documentation of red spruce growth decline. Canadian Journal of Forest Research **15**:1199-1201.

Huete, A., C. Justice, and H. Liu. 1994. Development of vegetation and soil indices for MODIS-EOS. Remote Sensing of Environment **49**:224-234.

Hunt, E. R. and B. N. Rock. 1989. Detection of changes in leaf water content using near- and middle-infrared reflectances. Remote Sensing of Environment **30**:43-54.

Innes, J. L. 1993. Forest health: Its assessment and status. CAB International Wallingford, Oxon, U.K.

Iverson, L. R. and A. M. Prasad. 1998. Predicting abundance of 80 tree species following climate change in the eastern United States. Ecological Monographs **68**:465-485.

Kaufmann, R. K., R. D. D'Arrigio, L. F. Paletta, H. Q. Tian, W. M. Jolly, and R. B. Myeni. 2008. Identifying climatic controls on ring width: The timing of correlations bewteen tree rings and NDVI. Earth Interactions **12**:1-12.

Kaufmann, R. K., R. D. D'Arrigo, C. Lakowski, R. B. Myneni, and L. Zhou. 2004. The effect of growing season and summer greenness on northern forests. Geophysical Research Letters **31**:LO9205.

Kessler, W. R. 2008. Spectral Effects of a Calcium Amendment on Red Spruce Foliage at Laboratory and Stand Scale. University of New Hampshire, Durham.

Kleinbaum, D. G., L. Kupper, M. K.E., and A. Nizam, editors. 1998. Applied Regression Analysis and Other Multivariable Methods. Cole Publishing, Inc., Pacific Grove, Ca.

Klos, R. J., G. G. Wang, W. L. Bauerle, and J. R. Rieck. 2009. Drought impact on forest growth and mortality in the southeast USA: an analysis using Forest Health and Monitoring data. Ecological Applications **19**:699-708.

Kosiba, A. M., P. G. Schaberg, G. J. Hawley, and C. F. Hansen. in review. Quantifying the influence of winter injury on the carbon sequestration of red spruce trees in the northeastern United States.

Kozak, A. and R. Kozak. 2003. Does cross validation provide additional information in the evaluation of regression models? Canadian Journal of Forest Research **33**:976-987.

Kulakowski, D., T. T. Veblen, and P. Bebi. 2003. Effects of fire and spruce beetle outbreak legacies in the disturbance regime of a subalpine forest in Colorado. Journal of Biogeography **30**:1445-1456.

Lloyd, A. H., A. G. Bunn, and L. T. Berner. 2010. A latitudinal gradient in tree growth response to climate warming in the Siberian taiga. Global Change Biology **17**:1935-1945.

Lopatin, E., T. Kolstrom, and H. Spiecker. 2006. Determination of forest growth trends in Komi Republic (northwestern Russia): combination of tree-ring analysis and remote sensing data. Boreal Environmental Research **11**:341-353.

Lovett, G. M., C. D. Canham, M. A. Arthur, K. C. Weathers, and R. D. Fitzhugh. 2006. Forest Ecosystem Responses to Exotic Pests and Pathogens in Eastern North America. BioScience **56**:395-405.

Malmström, C. M., M. V. Thompson, G. P. Juday, S. O. Los, J. T. Randerson, and C. B. Field. 1997. Interannual variation in global-scale net primary production: Testing model estimates. Global Biogeochem. Cycles **11**:367-392.

Martin, M. E. 1994. Measurements of foliar chemistry using laboratory and airborne high spectral resolution visible and infrared data. University of New Hampshire, Durham, NH, USA

Maselli, F. 2004. Monitoring forest conditions in a protected Mediterranean coastal area by the analysis of multiyear NDVI data. Remote Sensing of Environment **89**:423-433.

Maxwell, K. and G. N. Johnson. 2000. Chlorophyll fluorescence—a practical guide. Journal of Experimental Botany **51**:659-668.

Meng, Q., C. Cieszewski, and M. Madden. 2009. Large area forest inventory using Landsat ETM+: A geostatistical approach. ISPRS Journal of Photogrammetry and Remote Sensing **64**:27-36.

Mohammed, G. H., W. D. Binder, and S. L. Gillies. 1995. Chlorophyll fluorescence: A review of its practical forestry applications and instrumentation. Scandinavian Journal of Forest Research **10**:383-410.

Myeong, S., D. J. Nowak, and M. J. Duggin. 2006. A temporal analysis of urban forest carbon storage using remote sensing. Remote Sensing of Environment **101**:277-282.

Nakane, K. and Y. Kimura. 1992. Assessment of pine forest damage by blight based on Landsat TM data and correlation with environmental factors. Ecological Research **7**:9-18.

Niklasson, M. and A. Granstrom. 2000. Numbers and sizes of fires: Long-term spatially explicit fire history in a swedish boreal landscape. Ecology **81**:1484-1499.

North East State Foresters Association. 2007. The Economic Importance and Wood Flows from the Forests of Maine, New Hampshire, Vermont and New York, 2007. North East State Forester's Association.

Olson, M. G. 2011. Remote sensing of forest health trends in the northern Green Mountains of Vermont. University of Vermont, Burlington.

Olthof, I., D. J. King, and R. A. Lautenschlager. 2004. Mapping deciduous forest ice storm damage using Landsat and environmental data. Remote Sensing of Environment **89**:484-496.

Peñuelas, J., F. Baret, and I. Filella. 1995. Semi-empirical indices to asess carotenoids/chlorophyll a ratio from leaf spectral reflectance. Photosynthetica **31**:221-230.

Peñuelas, J., C. Field, K. Griffin, and J. Gamon. 1993. Assessing community type, plant biomass, pigment composition and photosynthetic efficiency of aquatic vegetation from spectral reflectance. Remote Sensing of Environment **46**:1-25.

Pierce, L. L., S. W. Running, and G. A. Riggs. 1990. Remote detection of canopy water stress in coniferous forests using the NS001 Thematic Mapper Simulator and the Thermal Infrared Multispectral Scanner. Photogrammetric Engineering and Remote Sensing **56**:579-586.

Pontius, J., R. A. Hallett, and M. E. Martin. 2005. Assessing hemlock decline using hyperspectral imagery: signature analysis, indices comparison and algorithm development Journal of Applied Spectroscopy **59**:836-843.

Pontius, J. A. in Review. A hyperspectral approach to multi-spectral forest decline assessments.

Pontius, J. A., M. E. Martin, M. G. Olson, K. M. White, W. L. Young, and E. M. D. Regan. in prep. Forest health trends in the Northeastern United States: a 25 year Landsat TM assessment.

Potter, C., P. Gross, V. Genovese, and M. L. Smith. 2007. Net primary productivity of forest stands in New Hampshire estimated from Landsat and MODIS satellite data. Carbon balance and management **2**:9.

Rock, B. N., J. E. Vogelmann, D. L. William, A. F. Vogelmann, and T. Hoshizaki. 1986. Remote detection of forest damage. BioScience **36**:439-445.

Rondeaux, G., M. Steven, and F. Baret. 1996. Optimization of soil-adjusted vegetation indices. Remote Sensing of Environment **55**:95-107.

Schaberg, P. G., B. E. Lazarus, G. J. Hawley, J. M. Halman, C. H. Borer, and C. F. Hansen. 2011. Assessment of weather-associated causes of red spruce winter injury and consequences to aboveground carbon sequestration. Canadian Journal of Forest Research **41**.

Seymour, R. S., A. S. White, and P. G. deMaynadier. 2002. Natural disturbance regimes in northeastern North America—evaluating silvicultural systems using natural scales and frequencies. Forest Ecology and Management **155**:357-367.

Siccama, T. G., M. Bliss, and H. W. Vogelmann. 1982. Decline of Red Spruce in the Green Mountains of Vermont. Bulletin of the Torrey Botanical Club **109**:162-168.

Sims, D. A. and J. A. Gamon. 2002. Relationships between leaf pigment content and spectral reflectance across a wide range of species, leage structures and developmental stages. Remote Sensing of Environment **81**:337-354.

Sivanpillai, R., C. T. Smith, R. Srinivasan, M. G. Messina, and X. B. Wu. 2006. Estimation of managed loblolly pine stand age and density with Landsat ETM+ data. Forest Ecology and Management **223**:247-254.

Smith, K. T. and W. C. Shortle. 2003. Radial growth of hardwoods following the 1998 ice storm in New Hampshire and Maine. Canadian Journal of Forest Research **33**:325-329.

Song, C., C. E. Woodcock, K. C. Seto, M. P. Lenney, and S. A. Macomber. 2001. Classification and Change Detection Using Landsat TM Data: When and How to Correct Atmospheric Effects? Remote Sensing of Environment **75**:230-244.

Spanner, M. A., L. L. Pierce, D. L. Peterson, and S. W. Running. 1990. Remote sensing of temperate coniferous forest leaf area index The influence of canopy closure, understory vegetation and background reflectance. International Journal of Remote Sensing **11**:95-111.

Speer, J. H. 2010. Fundamentals of Tree-ring Research. The University of Arizona Press, Tucson, AZ.

Speer, J. H., K. Clay, G. Bishop, and M. Creech. 2010. The effect of periodical cicadas on growth of five tree species in midwestern deciduous forests. The American Midland Naturalist **164**:173-186.

Speer, J. H., T. W. Swetnam, B. E. Wickman, and A. Youngblood. 2001. Changes in pandora moth outbreak dynamics during the past 622 years. Ecology **83**:679-697.

Stahle, D. W., M. K. Cleaveland, D. B. Blanton, M. D. Therrell, and D. A. Gay. 1998. The Lost Colony and Jamestown Droughts. Science **280**:564-567.

Stahle, D. W., F. K. Fye, E. R. Cook, and D. Griffin. 2007. Tree-ring reconstructed megadroughts over North America since A.D. 1300. Climatic Change **83**:133-149.

Stein, S. M., R. E. McRoberts, L. G. Mahal, M. A. Carr, R. J. Alig, S. J. Comas, D. M. Theobald, and A. Cundiff. 2009. Private Forests, Public Benefits: Increased Housing Density and Other Pressures on Private Forest Contributions. USDA Forest Service Pacific Northwest Research Station.

Stokes, M. A. and T. L. Smiley. 1968. An Introduction to Tree-Ring Dating. University of Chicago Press, Chicago.

Sutton, A. and J. C. Tardis. 2007. Dendrochronological reconstruction of forest tent caterpillar outbreaks in time and space, western Manitoba, Canada. Canadian Journal of Forest Research **37**:1643-1657.

Swetnam, T. W. and C. H. Baisan. 1996. Fire Histories of the Montane Forests in the Madrean Boderlands. USDA, Forest Service.

Townsend, P. A., A. Singh, J. R. Foster, N. J. Rehberg, C. C. Kingdon, K. N. Eshleman, and S. W. Seagle. 2012. A general Landsat model to predict canopy defoliation in broadleaf deciduous forests. Remote Sensing of Environment **119**:255-265.

Vermont Department of Forests, Parks and Recreation,. 2010. 2010 Vermont Forest Resources Plan., Vermont Agency of Natural Resources, Montpelier, VT.

Vogelmann, J. E. and B. N. Rock. 1988. Assessing forest damage in high-elevation coniferous forests in vermont and new Hampshire using thematic mapper data. Remote Sensing of Environment **24**:227-246.

Vogelmann, J. E. and B. N. Rock. 1989. Use of Thematic Mapper data for the detection of forest damage caused by pear thrips. Remote Sensing of Environment **30**:217-225.

Vogelmann, J. E., B. N. Rock, and D. M. Moss. 1993. Red edge spectral measurements from sugar maple leaves. International Journal of Remote Sensing **14**:1563-1575.

Vogelmann, J. E., B. Tolk, and Z. Zhu. 2009. Monitoring forest changes in the southwestern United States using multitemporal Landsat data. Remote Sensing of Environment **113**:1739–1748.

Wang, J., P. M. Rich, K. P. Price, and W. D. Kettle. 2004. Relations between NDVI and tree productivity in the central Great Plains. International Journal of Remote Sensing **25**:3127-3138.

Wargo, P. M. and A. N. D. Auclair. 2000. Forest declines in response to environmental change. Pages 117-145 *in* R. A. Mickler, R. A. Birdsey, and J. Hom, editors. Responses of northern U.S. forests to environmental change. Ecological Studies 139. Springer-Verlag, New York.

Williams, P. and K. Norris. 2001. Near-Infrared Technology in the Agricultural and Food Industries. American Association of Ceral Chemists, Inc., St. Paul, MN.

Wolter, P. T., P. A. Townsend, B. R. Sturtevant, and C. C. Kingdon. 2008. Remote sensing of the distribution and abundance of host species for spruce budworm in Northern Minnesota and Ontario. Remote Sensing of Environment **112**:3971-3982.

Wyckoff, P. H. and J. S. Clark. 2002. The Relationship between Growth and Mortality for Seven Co-Occurring Tree Species in the Southern Appalachian Mountains. Journal of Ecology **90**:604-615.

Yamaguchi, D. K. 1991. A simple method for cross-dating increment cores from living trees. Canadian Journal of Forest Research **21**:414-416.

Zhang, L., B. D. Rubin, and P. D. Manion. 2011. Mortality: the essence of a healthy forest. Pages 17-49 *in* J. D. Castello and S. A. Teale, editors. Forest Health, An Integrated Perspective. University Press, Cambridge, UK.